ISTANBUL TECHNICAL UNIVERSITY ★ GRADUATE SCHOOL

MOLECULAR DYNAMICS INVESTIGATION OF THE EFFECTS OF F318L MUTATION ON YEAST HOG1 PROTEIN

M.Sc. THESIS

Altuğ ULUDAĞ

Department of Molecular Biology-Genetics and Biotechnology

Molecular Biology-Genetics and Biotechnology Programme

MARCH 2024

ISTANBUL TECHNICAL UNIVERSITY ★ GRADUATE SCHOOL

MOLECULAR DYNAMICS INVESTIGATION OF THE EFFECTS OF F318L MUTATION ON YEAST HOG1 PROTEIN

M.Sc. THESIS

Altuğ ULUDAĞ
(521191102)

Department of Molecular Biology-Genetics and Biotechnology

Molecular Biology-Genetics and Biotechnology Programme

Thesis Advisor: Assist. Prof. Dr. Bülent BALTA

MARCH 2024

İSTANBUL TEKNİK ÜNİVERSİTESİ ★ LİSANSÜSTÜ EĞİTİM ENSTİTÜSÜ

F318L MUTASYONUNUN MAYA HOG1 PROTEİNİ ÜZERİNDEKİ ETKİLERİNİN MOLEKÜLER DİNAMİK ARAŞTIRMASI

YÜKSEK LİSANS TEZİ

Altuğ ULUDAĞ
(521191102)

Moleküler Biyoloji-Genetik ve Biyoteknoloji Bölümü

Moleküler Biyoloji-Genetik ve Biyoteknoloji Programı

Tez Danışmanı: Dr. Öğretim Üyesi Bülent BALTA

MART 2024

Altuğ ULUDAĞ, a M.Sc. student of İTU Graduate School student ID 521191102 successfully defended the thesis/dissertation entitled "MOLECULAR DYNAMICS INVESTIGATION OF THE EFFECTS OF F318L MUTATION ON YEAST HOG1 PROTEIN", which he prepared after fulfilling the requirements specified in the associated legislations, before the jury whose signatures are below.

Thesis Advisor :	**Assist. Prof. Dr. Bülent BALTA** İstanbul Technical University	.....
Jury Members :	**Prof. Dr. Zeynep Petek ÇAKAR** Istanbul Technical University	.....
	Prof. Dr. Safiye ERDEM Marmara University	.....

Date of Submission : 26 May 2023
Date of Defense : 05 March 2024

To my dad and family,

FOREWORD

First of all, I would like to thank Assit. Prof. Dr. Bülent Balta for his guidance throughout this study. His experience and expertise illuminated the path to writing this thesis.

Second, I would like to thank TRUBA and UHEM supercomputing centers, who provided support to computational research. The numerical calculations reported in this thesis were partially performed at TUBITAK ULAKBIM, High Performance and Grid Computing Center (TRUBA resources) and UHEM.

The most special thanks are to my family, my dad and mom, without whom I wouldn't be who I am.

Special thanks to my wife, for standing by me throughout our life. You are making my life more fun and tolerable.

Life withouth friends are just boredom. I am grateful to have such friends, with whom I feel happy and valuable. Brothers not by mother but by heart, dear Onur, I am lucky to have you on my side through my life. Little brother that I never had but I'll always have, dear İsmail, deepest thanks to you both your effort in this project and for our relationship. Dear Ayşe Buse, your company and support during every part of my life is extremely important, and I'm thankful to have you in my life. And Osman, my dearest bro, thanks for all the great moments that we have and we will have.

Lastly, Dear Öykü, the big sister, thank you for being a part of my life. You are always teaching me different aspects of life that I'm not aware of.

And before closing, Prof. Dr. Fatma Neşe KÖK, I would like to thank you for all the efforts that you put forth during our time together.

March 2024 Altuğ ULUDAĞ

TABLE OF CONTENTS

Page

ABBREVIATIONS

ERK	**:** Extracellular signal-regulated kinase
HOG1	**:** High Osmolarity Glycerol response 1
JNK	**:** c-Jun N-terminal kinase
MAPK	**:** Mitogen activated protein kinase
MAPKK	**:** Mitogen activated protein kinase kinase
MAPKKK	**:** Mitogen activated protein kinase kinase kinase
ns	: Nanoseconds
PKC	**:** Protein kinase C
ps	: Picoseconds

SYMBOLS

$\sum$	**:** Sum
θ	**:** Angle between atoms
ϕ	**:** Dihedral angle
δ	**:** Dihedral angle where torsion angle is minimum
q	**:** Charge of atoms
μs	: Microseconds
K	: Kelvin
$\mathbf{V_n}$	: Rotational barrier height
Å	: Angstrom
$\mathbf{K^+}$	: Potassium ion

LIST OF TABLES

Page

LIST OF FIGURES

Page

MOLECULAR DYNAMICS INVESTIGATION OF THE EFFECTS OF F318L MUTATION ON YEAST HOG1 PROTEIN

SUMMARY

Environmental stress is a key factor affecting cell function and viability for all living organisms. Organisms have developed several mechanisms to cope with stress conditions. *Saccharomyces cerevisiae* activates Hog1 protein through a MAPK cascade, which results with resistance to high osmolarity environment under osmotic stress conditions.

Activation of Hog1 is regulated by its upstream kinases and causes its translocation to nucleus and affect transcription of several genes. Some mutations on the Hog1 protein lead to a constitutive activation of the protein, which eliminates the need of its kinase to activate Hog1. F318L mutation is one of the activating mutations discovered on Hog1 protein. Mechanism of protein activation due to F318L mutation was investigated in this study using molecular dynamics simulations.

First, structure of Hog1 is predicted using Alphafold Protein Structure Database since Hog1 does not have a crystal structure. After preparation of initial structure belonging to wild-type unphosphorylated, nucleotide-free protein is obtained, predicted structures were taken and compared with known MAPK crystal structures, 1erk and 2erk.

Second, alternative structures were prepared to mimic each possible form that protein can take. These alternative structures comprise of two groups namely wild-type and mutant Hog1 and their combinations as unphosphorylated, dual phosphorylated, nucleotide-free and ATP bound models. After serveral simulation, two additional different starting geometries were introduced.

We found that the position of L165, which is thought to guide the substrate in the active site is affected by the mutation, phosphorylation or the presence of ATP. In simulations where L165 cannot interact with a hydrophobic cluster consisting of L73, F318 and W320, the active site is mostly in closed conformation, unreachable by the substrate. I168 interacts with the hydrophobic cluster. This arrangement blocks L165 from reaching the hydrophobic cluster, locating it next to the ATP binding site. When T174 and Y176 are phosphorylated, active site also opened up, allowing downstream processes to occur. In mutant model, L165 interacts with L73 and L318, leaving the active site open. When ATP is present in unphosphorylated mutant model, it repositioned itself in a different geometry, which allowed it to form a potentially catalytic interaction with R66.

Investigation of effects of F318L mutation on yeast Hog1 protein by the use of computational chemistry methods is the aim of this study.

F318L MUTASYONUNUN MAYA HOG1 PROTEİNİ ÜZERİNDEKİ ETKİLERİNİN MOLEKÜLER DİNAMİK ARAŞTIRMASI

ÖZET

Çevresel stres, tüm canlı organizmalar için hücre işlevini ve canlılığını etkileyen önemli bir faktördür. Organizmalar stres koşullarıyla başa çıkmak için çeşitli mekanizmalar geliştirmiştir. *Saccharomyces cerevisiae*, ozmotik stres koşulları altında yüksek ozmolarite ortamına dirençle sonuçlanan bir MAPK kaskadı yoluyla Hog1 proteinini aktive eder.

MAPK protein aileleri aralarında dizi benzerlikleri ve korunmuş yapılara sahiptir. Maya Hog1 proteininin üç boyutlu kristal yapısı olmasa da MAPK ailesinin bir üyesi olarak diğer MAPK'ler arasında korunmuş yapılara sahiptir. Aktif bölge bir nükleotit bağlanma bölgesi ile fosforilasyon dudağı adı verilen ve fosforilasyon hedefi olan Thr174 ve Tyr176 kalıntılarını içeren bir döngüden oluşur.

Ozmotik stres koşulları altında Hog1, Thr174 ve Tyr176 kalıntıları üzerindeki ikili fosforilasyon yoluyla üst kinazı tarafından aktive edilir. Hog1'in iki kalıntı üzerindeki fosforilasyonu, aktivitesini önemli ölçüde artırır. Çalışmalar, Hog1'deki Tyr176 ve Thr174 kalıntıları üzerindeki ikili mutajenezin, hücrelerin yüksek ozmolariteli ortamlarda büyüyememesine yol açtığını göstermektedir. Tyr176 kalıntısının alanine mutajenezi hücrelerin ozmotik stres altında büyüme yeteneğini etkilemezken, Thr174 kalıntısının fenilalanine değiştirilmesi hücrelerin stres koşulları altında hayatta kalma yeteneğini önemli ölçüde azaltır. Böylece Thr174 kalıntısının Hog1 aktivitesi için kritik olduğu gösterilmiştir. Ayrıca Hog1-F318L gibi aktif Hog1 mutantlarının üst kinazının yokluğunda düşük seviyelerde fosforilasyon gösterdiği belirtilmiştir.

Hog1'in aktivasyonu, üst kinazları tarafından düzenlenir ve çekirdeğe translokasyonuna neden olur ve birkaç genin transkripsiyonunu etkiler. Hog1 proteini üzerindeki bazı mutasyonlar, kinazının Hog1'i aktive etme ihtiyacını ortadan kaldırır ve proteinin sürekli aktivasyonuna yol açar. F318L mutasyonu, Hog1 proteininde keşfedilen aktive edici mutasyonlardan biridir.

Moleküler dinamik, sistemlerin davranışını ve dinamiklerini atom düzeyinde araştırmak için kullanılan güçlü bir hesaplama tekniğidir. Atomların ve moleküllerin zaman içinde nasıl hareket ettiği ve etkileşime girdiğinin ayrıntılı bir şekilde anlaşılmasını sağlar. Moleküler dinamik, parçacıkların hareketini klasik mekanik prensiplerine göre simüle ederek, bilim adamlarının deneysel olarak incelenmesi zor olan karmaşık proteinlerin özelliklerini ve davranışlarını keşfetmesine olanak tanır.

Moleküler dinamik simülasyonlarında sistemin yörüngesi, Newton'un hareket denklemlerinin sayısal olarak entegre edilmesiyle oluşturulur. Başlangıçta sisteme enerjisine göre bir kuvvet uygulanır ve ardından atomların koordinatları hesaplanır. Bu süreç, bir kuvvet alanı veya potansiyel enerji fonksiyonu tarafından tanımlanan atomlar arası etkileşimleri hesaba katarak, her bir atoma etki eden kuvvetlerin değerlendirilmesini içerir. Atomlara uygulanan kuvvetler onların ivmesini belirler ve bu da onların hızlarını etkiler.

Atomların yeni hızları türetildikten sonra, her bir atomun yer değiştirmesi, mevcut hızına ve bir zaman adımına göre hesaplanır. Bu yer değiştirme daha sonra atomların koordinatlarını güncellemek için kullanılır. Bu hesaplamaların düzenli aralıklarla tekrarlanmasıyla sistemin davranışı zaman içinde takip edilebilir, dinamik özellikleri ortaya çıkarılabilir ve çeşitli fiziksel olayların gözlemlenmesine olanak sağlanır.

Moleküler dinamik simülasyonları çok çeşitli bilimsel sorulara değerli bilgiler sağlar. Proteinlerin katlanma mekanizmalarını, enzimlerin davranışlarını, ilaç molekülleri ile reseptör arasındaki etkileşimleri aydınlatabilirler. Bilim adamları, moleküler dinamik tarafından oluşturulan yörüngelerin analizi yoluyla termodinamik özellikler, yapısal değişiklikler, reaksiyon mekanizmaları ve difüzyon hızları gibi önemli bilgiler elde edebilirler.

Fosforilasyon bölgesi, ATP bağlanma bölgesi ve mutasyon bölgesini (F318/L318) içeren hidrofobik bir küme bu çalışmanın ana odak noktasıdır çünkü bu alanlar mutasyon, nükleotid bağlanması ve fosforilasyondan etkilenir. ATP yokluğunda, fosforile edilecek kalıntılardan biri olan Y176 aktif bölgenin girişini kapatmaktadır. Fosforilasyonun diğer hedefi olan T174, aktif bölgenin uzağında konumlanmıştır. T174 ve Y176'nın pozisyonları, fosforile edilmemiş insan Erk2 ve p38 kristallerindeki (PDB kodları: 1erk ve 1wfc) karşılıklarına benzemektedir. Dolayısıyla dudağın konformasyonu literatürde fosforile edilmemiş MAP kinazlarda da bulunan kapalı bir konformasyondur. Substratı yönlendirdiği düşünülen L165, N149 ve D162 ile işaretlenen ATP bağlanma bölgesinin yanında yer alır. T174 ve Y176, fosforile edildiklerinde bu iki amino asitle etkileşime girme potansiyeline sahip altı arjinin kalıntısı ile çevrelenmiştir.

Mutasyon hidrofobik kümede bulunduğundan bu bölgedeki organizasyonun net bir şekilde belirlenmesi önemlidir. Bu nedenle, yabanıl tip ve mutant sistemlerin her biri için, W320 veya F322'nin yönelimi değiştirilerek alternatif başlangıç geometrileri hazırlanmıştır. W320 yan zinciri hidrofobik kümeden solvente doğru döndürülmüştür. F322 yan zinciri F359'a doğru yeniden yönlendirildi.

Mutant başlangıç geometrileri, F318'in manuel olarak lösine dönüştürülmesiyle tasarlanmıştır. Yukarıda açıklanan hidrofobik kümenin üç düzenlemesinin her biri için mutant yapılar hazırlanmıştır.

Fosforile edilmiş sistemler, Alphafold'dan alınan yapıdaki hem T174 hem de Y176'ya fosfat gruplarının manuel olarak eklenmesiyle elde edilmiştir. Mutantlar fosforilasyon olmadan da yapısal olarak aktif olduğundan, bu çalışmada yalnızca yabanıl tip proteinler fosforilasyona tabi tutuldu.

Ayrıca yabanıl tipte, nükleotit içermeyen, fosforile edilmemiş bir sistemde 1 µs simülasyonun sonunda fosfat grupları eklenerek bir µs daha simüle edilmiştir. Bunun tersine, yabanıl tipte, nükleotid içermeyen, fosforile edilmiş bir sistemde 1 µs simülasyonun sonunda fosfat grupları çıkarıldı ve bir µs daha simüle edildi. Son olarak mutant, nükleotid içermeyen, fosforile edilmemiş bir sistem 1 µs sonunda yabanıl tipe dönüştürülmüş ve bir µs daha simüle edilmiştir.

Alphafold'un verdiği yapı 1wfc ve 1atp kristal yapılarına benzerdir. 1atp kristalinde bir substrat analoğu vardır. Substrat analoğundaki alanin, substrattaki treonin veya serin olacaktır. Bu kalıntı, Hog1'deki Leu165'in eşdeğeri olan Phe187 ile ATP arasındadır. Alphafold yapımızda L165, 1atp'de F187 ile aynı konumdadır. 1wfc'de L74, Y323 ile hidrofobik etkileşimler yapmaktadır. Alphafold yapıda aynı pozisyonda L73 ve F318 amino asitleri bulunmakta ve kristal yapılar ile aynı etkileşimlere

sahiplerdir. Yabanıl tip fosforilasyonlu yapıdaki W320, nükleotid içermeyen (WT) yapıda olduğu gibi, 2 μs civarında solvente dönmektedir.

Substratı aktif bölgede yönlendirdiği düşünülen L165'in pozisyonunun mutasyon, fosforilasyon veya ATP varlığından etkilendiği bulunmuşturç. L165'in L73, F318 ve W320'den oluşan hidrofobik bir kümeyle etkileşime giremediği simülasyonlarda aktif bölge çoğunlukla etkileşim partnerleri tarafından erişilemeyen kapalı konformasyondadır. I168 hidrofobik kümeyle etkileşime girmektedir. Bu düzenleme, L165'in hidrofobik kümeye ulaşmasını engelleyerek onu ATP bağlanma bölgesinin yanına yerleştirir. T174 ve Y176 fosforile edildiğinde aktif bölge de açılarak aşağı yönlü süreçlerin gerçekleşmesine olanak tanmaktadır. Mutant modelde L165, L73 ve L318 ile etkileşime girerek aktif bölgeyi açık bırakmaktadır. Fosforile edilmemiş mutant modelde ATP mevcut olduğunda, kendisini farklı bir geometride yeniden konumlandırmıştır ve bu da R66 ile potansiyel olarak katalitik bir etkileşim oluşturmasına izin vermektedir.

Özetlemek gerekirse, fosforile edilmemiş yabanıl tip modelde L165, ATP mevcut olduğunda aktif bölgeye çok uzak, ancak ATP mevcut olmadığında çok yakındır. Fosforilasyon, L165'in doğru şekilde konumlandırılmasına hizmet edebilir. Mutant, L165'i hidrofobik kümede konumlandırabilir, G164'ü L165'in yan zincirinin ATP'siz yabanıl tipteki modelde bulunduğu yerde konumlandırabilir ve ATP'yi farklı bir yönelimde konumlandırarak onu reaksiyon için uygun hale getirebilir.

Bu modeller diğer organizmalardaki mekanizmaların anlaşılmasına yönelik veriler sağlayabilir. Mutant proteini manipüle etmek için farklı mühendislik yöntemleri geliştirilebilir, bu da gerektiğinde etkinleştirmemize veya devre dışı bırakmamıza olanak tanır. Ayrıca, kurucu aktivasyon mekanizmasının anlaşılmasıyla önleyici mekanizmalar veya substratlar geliştirilebilir.

F318L mutasyonunun maya Hog1 proteini üzerindeki etkilerinin hesaplamalı kimya yöntemleri kullanılarak araştırılması bu çalışmanın amacını oluşturmaktadır.

1. INTRODUCTION

Osmotic stress affects cellular mechanisms and cell viability. Cells activate or deactivate several pathways to protect themselves against osmotic changes in the world they live in. Hog1 is a protein found in *S. cerevisiae* which is activated by its kinase to cope with osmotic stress. Among several mutations found in Hog1 protein, F318L mutation causes protein to remain active constitutively, without the need for its kinase to activate Hog1. I will investigate the effect of F318L mutation on constitutive activation of Hog1 in this thesis study.

1.1 Osmotic Stress

Living organisms encounter multiple environmental stresses throughout their life cycle, and alterations in osmolarity represent one such challenge that can profoundly influence their growth, survival, and overall fitness. In response to these changes, cells have developed complicated mechanisms to sense and respond to osmotic stress. The model organism *Saccharomyces cerevisiae* has a regulatory network with several important participants. One of these participants is the highly conserved protein Hog1 (High Osmolarity Glycerol response 1), which plays a key role. Hog1 serves as a critical mediator of the cellular response to osmotic stress, orchestrating a series of coordinated events that enable cells to maintain cytoplasmic stability and adapt to diverse external osmolarities (Blomberg, 2022).

1.2 MAPK Cascade in Yeast

Multiple cascades of mitogen-activated protein kinases (MAPKs) exist in eukaryotic cells and are responsible for appropriate cellular responses to specific environmental signals (Robinson and Cobb, 1997; Banuett, 1998). In metazoans, yeast, and other organisms, MAPK pathways are involved in growth, development, and stress responses. In specific organisms like *Drosophila, Caenorhabditis elegans*, and vertebrates, receptor tyrosine kinases activate MEK and MAPK through Ras and Raf, regulating growth and development. In vertebrates, similar kinases such as JNK/SAPK

and p38 regulate stress responses. In *Saccharomyces cerevisiae*, six distinct MAPK signaling pathways control mating, pseudohyphal growth, invasiveness, cell wall biosynthesis, osmotic stress response, and spore wall formation. These pathways involve a module consisting of two kinases, MEK and MAPK. MEK is activated through phosphorylation of specific serine and threonine residues and, in turn, activates MAPK by phosphorylating specific threonine and tyrosine residues in a region called the phosphorylation lip. The MAPK cascade comprises three components: a MAPK, a MAPK kinase (MAPKK), and a MAPKK kinase (MAPKKK). In *Saccharomyces cerevisiae*, four complete MAPK cascade modules have been identified (Herskowitz, 1995; Levin and Errede, 1995). The pheromone response pathway is activated by peptide pheromones and facilitates mating preparation in cells (Leberer et al., 1997). The pseudohyphal development/invasive growth pathway responds to environmental conditions, allowing the formation of pseudohyphal cells in diploids and invasive growth in haploids (Liu et al., 1993; Roberts and Fink, 1994). The PKC-regulated MAPK pathway responds to heat stress and hypotonic shock (Davenport et al., 1995; Kamada et al., 1995), while the high osmolarity glycerol (HOG) pathway responds to hypertonic stress (Brewster et al., 1993).

The MAPKKK Ste11p plays a crucial role in three yeast MAPK pathways: the pheromone response pathway, the pseudohyphal/invasive growth pathway, and the HOG pathway (Dietzel and Kurjan, 1987; Miyajima et al., 1987).

1.3 High Osmolarity Glycerol response 1

MAPK1 refers to a wide group of enzymes that play a role in various pathways involved in signal transduction. In mammals, these MAPKs can be classified into distinct subfamilies, namely ERKs, p38s, and JNKs, based on their level of similarity, biological functions, and phosphorylation patterns. Despite their structural and activation similarities, each MAPK responds to specific signals and phosphorylates specific substrates, leading to distinct cellular effects.

Saccharomyces cerevisiae has five MAPKs that are similar to their mammalian counterparts. Fus3, Kss1, and Mpk1 MAPKs in yeast share close similarities with the ERK subfamily found in mammals. The Hog1 MAPK in yeast has a phosphorylation motif (QM*TG*YVSTR) that is nearly identical to that of p38 MAPK in mammals,

and it serves a similar functional role as either JNKs or p38s. Hog1 is activated through phosphorylation by the MAPKK Pbs2, which functions similarly to JNKK1/MKK4 in mammals. The Pbs2/Hog1 MAPK cascade plays a vital role in the survival of yeast cells under high osmotic conditions. Yeast cells lacking either Pbs2 or Hog1 are unable to grow on media containing elevated concentrations of sugar or salt (Westfall et al., 2008).

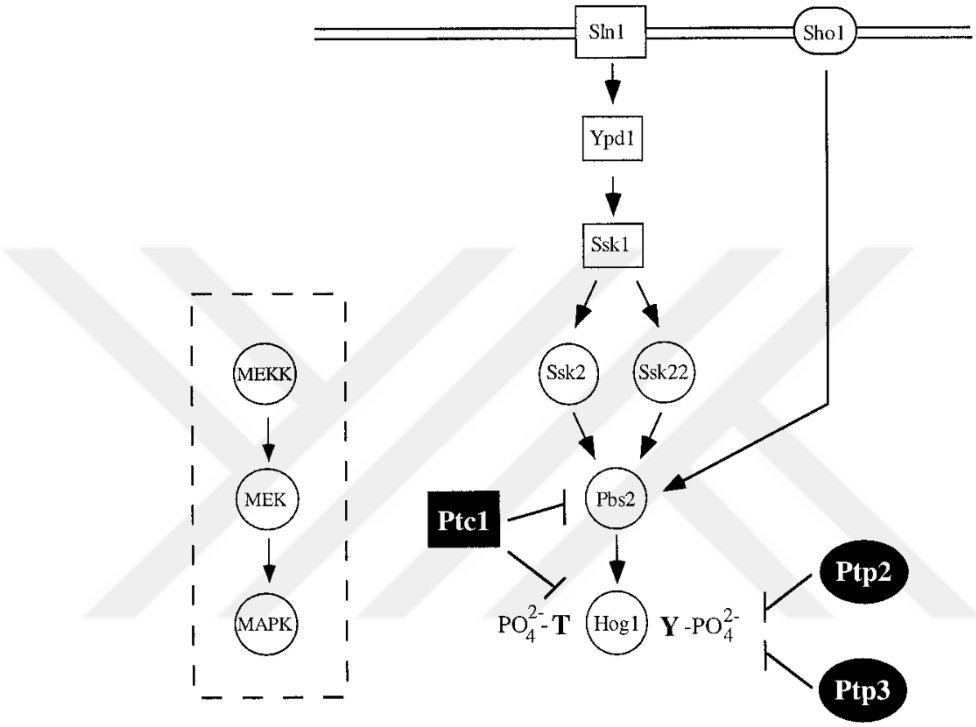

Figure 1.1: Osmotic stress response pathway in S. cerevisiae. Phospatases Ptc1, Ptp2 and Ptp3 negatively regulates the pathway, while cascade of kinases activates the Hog1 (Jacoby et al., 1997).

The activation of the MAPK, Hog1, in the HOG pathway is driven by two separate inputs (Figure 1). When the osmolarity of the environment is at equilibrium, a transmembrane protein-histidine kinase called Sln1 initiates a series of phosphorylation events involving multiple proteins, resulting in the inhibition of two closely related isoforms of the MAPKKK (Mitogen-Activated Protein Kinase Kinase Kinase), Ssk2 and Ssk22. However, when moderate levels of osmolytes are present (e.g., 0.1 to 0.4 M NaCl), Sln1's function is somehow blocked, leading to the relief of inhibition on Ssk2 and Ssk22. These enzymes then undergo phosphorylation and become active, subsequently phosphorylating and activating the MAPK kinase (MAPKK), Pbs2. Pbs2, in turn, phosphorylates both Thr174 and Tyr176 residues in Hog1, resulting in the activation of this MAPK (Jacoby et al., 1997).

1.4 Structure of Hog1 Protein

MAPK protein families have sequence similarities and conserved structures among them. Although not having a crystal structure, yeast Hog1 protein is a member of MAPK family, thus having conserved structures among other MAPKs. Active site comprises of a phosphorylation lip where phosphorylation of threonine and tyrosine residues occurs to activate the MAPK, a nucleotide binding region which allows ATP to bind and catalysis center in between. Below in Figures 1.2, 1.3 and 1.4 crystal structures of different MAPK proteins are given, which are later to be used in the formation of the initial structures and evaluation and verification of the final geometries.

Figure 1.2: Crystal structure of unphosphorylated, nucleotide-free Erk2 protein (pdb: 1erk) Phosphorylation lip is painted in orange.

Lip conformations are different among unphosphorylated MAPKs (Figure 1.2) and double phosphorylated MAPKs (Figure 1.3) to allow an open active site conformation upon phosphorylation event to activate the MAPK (Bellon et al., 1999; Canagarajah et al., 1997).

Nucleotide binding in MAPKs stabilized through asparagine and aspartate residues which are in close proximity to the ATP binding site. Mg^{2+} ions form a complex with ATP and bridges alpha and gamma phosphates (Zheng et al., 1993).

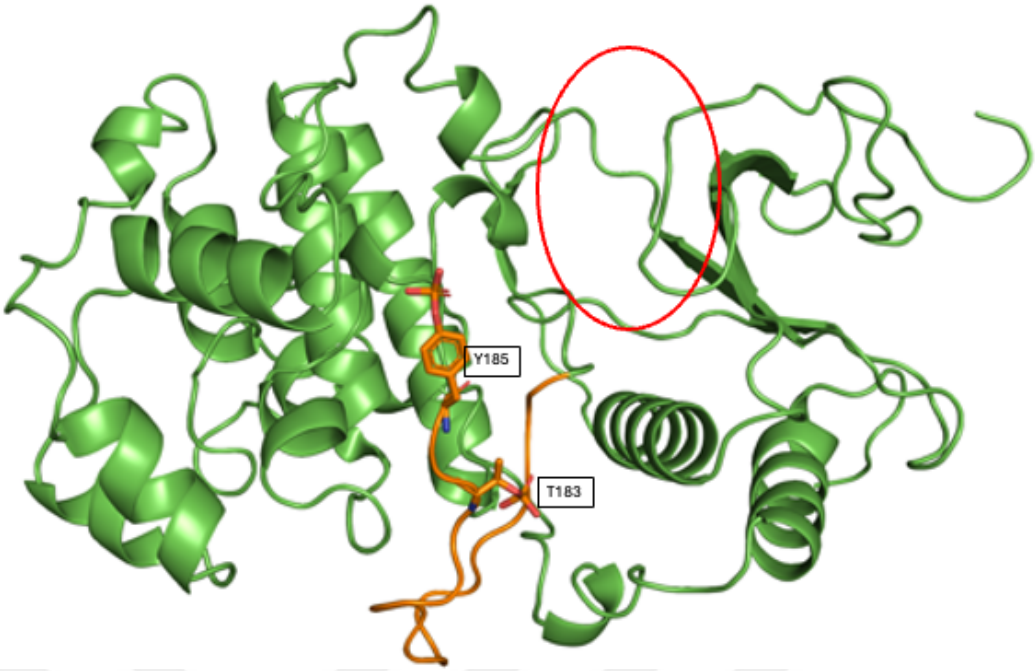

Figure 1.3: Crystal structure of double phosphorylated, nucleotide-free Erk2 protein (pdb: 2erk) Phosphorylation lip is painted in orange.ATP binding site is denoted with red circle.

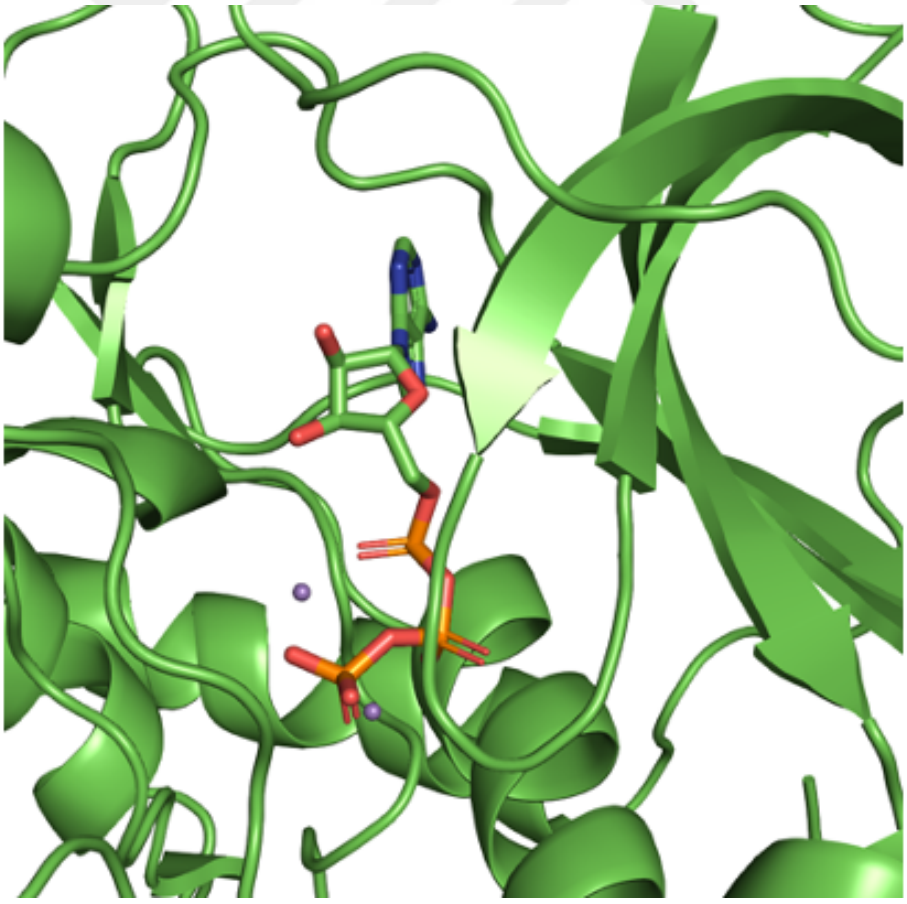

Figure 1.4: Crystal structure of unphosphorylated, ATP bound cAMP-dependent protein kinase protein (pdb: 1atp).

1.5 Hog1 in Osmotic Stress

S. cerevisiae, a unicellular eukaryotic organism commonly known as baker's yeast, has long served as an invaluable model system for understanding fundamental biological processes. It possesses a complicated osmoregulatory system that enables it to thrive in diverse osmotic conditions, including high salt concentrations. The protein Hog1 lies at the heart of this system, playing an important role in signaling the presence of osmotic stress and coordinating the cellular response.

Hog1 operates through a conserved mitogen-activated protein kinase (MAPK) signaling pathway, which is highly responsive to changes in external osmolarity. Under normal conditions, Hog1 remains inactive in the cytoplasm. However, when the osmolarity of the environment increases, the MAPK cascade is activated, leading to the phosphorylation and activation of Hog1. Once activated, Hog1 translocates to the nucleus, where it regulates the expression of target genes involved in osmoregulation, stress adaptation, and cell survival.

Under high osmotic conditions, yeast cells accumulate glycerol to counteract the osmotic differential between the cell interior and the external environment (Blomberg and Adler, 1992). This leads to the activation of the MAPK Hog1p, which stimulates increased glycerol synthesis by activating genes such as GPD1 (Larsson et al., 1993; Albertyn et al., 1994). The activation of Hog1 triggers a series of downstream events to restore cellular homeostasis.

Changes in the HOG pathway is given in Figure 1.5. Through the synthesis and accumulation of glycerol, an osmoprotectant, that helps maintain cellular turgor and prevents water loss which is the primary role of Hog1. Glycerol production is facilitated by the upregulation of enzymes involved in glycerol biosynthesis, including glycerol-3-phosphate dehydrogenase (GPD1/2) and glycerol-3-phosphatase (GPP2). Additionally, Hog1 influences the transcriptional regulation of numerous other genes involved in cell wall integrity, ion transport, protein folding, and stress response, thereby enabling the cell to adapt and withstand osmotic challenges (Blomberg, 2022).

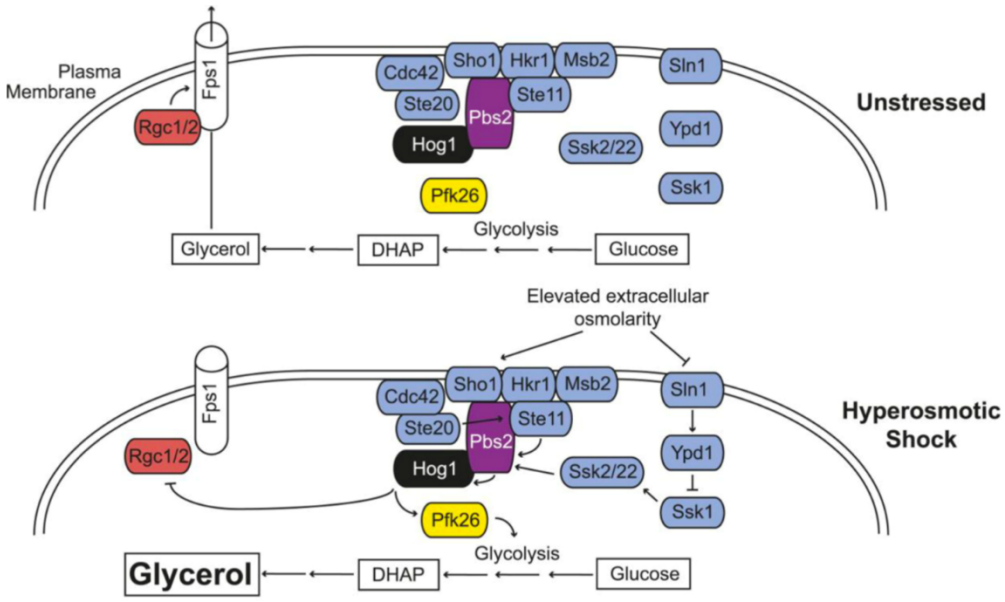

Figure 1.5: Role of Hog1 in osmotic stress. Hog1 is inactive, and glycerol is pumped out of cell in normal conditions. Upon activation in high osmolarity conditions, Hog1 activates and deactivates several proteins to increase the glycerol production and decrease the outflow (Blomberg, 2022).

1.6 Phosphorylation of Hog1

Under osmotic stress conditions, Hog1 is activated by its kinase through dual phosphorylation on residues T174 and Y176. Phosphorylation of Hog1 on two residues significantly increases its activity. Studies show that dual mutagenesis on the Y176 and T174 residues on Hog1, cells were unable to grow in high osmolarity environments. While mutagenesis of Y176 residue to alanine does not affect the ability of cells to grow under osmotic stress, changing T174 residue to phenyl alanine significantly reduces cells' ability to survive under stress conditions. Thus, T174 residue is shown to be critical for Hog1 activity. Furthermore, active Hog1 mutants such as Hog1-F318L showed low levels of phosphorylation in the absence of its kinase. Considering protein activity without the presence of its kinase, detection of low level phosphorylation, and loss of protein activity on Hog1 protein lacking the T174 residue, autophosphorylation of T174 residue could explain the mutant protein activity (Bell et al., 2001).

1.7 F318L Mutation in Hog1

The Hog1 protein comprises several functional domains that facilitate its signaling and regulatory functions. Of particular interest is the region around amino acid residue 318.

Studies have identified a missense mutation at this position, resulting in the substitution of a phenylalanine residue with leucine (F318L). This mutation changes the protein structure and causes its constitutive activation, potentially affecting its signaling properties.

It is known from previous studies that Hog1 operates downstream of a MAPKK cascade, where it is activated by dual phosphorylation on specific threonine and tyrosine residues. Once activated, Hog1 translocates to the nucleus and regulates gene expression, enabling cells to adapt to osmotic stress conditions. The F318L mutation activates the Hog1 protein in a constitutive manner, without the need for its kinase. However, the mechanism by which the F318L mutation affects Hog1 signaling remains largely unexplored (Bell et al., 2001).

Furthermore, in a recent study, evolutionary engineering is used to develop a stress resistant strain of *S. cerevisiae*. Evolutionary engineering, also known as inverse metabolic engineering, is a process that selects for desired traits in microorganisms. Unlike traditional methods, it uses systematic approaches like repeated batch or prolonged chemostat cultivations to induce mutations and select for fitter variants. First step increases genetic diversity using random mutagenesis and continues with targeted mutagenesis by exposing the organism to a selective pressure. This method has successfully improved various properties in important microorganisms like stress resistance, protein production, and metabolic activity. Evolutionary engineering mimics natural mutation processes and avoids introducing foreign genes. 2-phenylethanol, which is a widely used compound in cosmetic, perfume and food industries is used as external osmotic stress to induce mutations and led to F318L mutation on Hog1 protein. Also, these strains with mutant Hog1 protein shown increased resistance to osmotic stress, which supports the effect of the mutation (Çakar et al., 2011; Holyavkin et al., 2023). This recent study led us to study the mechanism and effects of constitutive activation of Hog1 protein through F318L mutation.

1.8 Aim of the Thesis

Hog1 protein plays a crucial role on osmotic stress response of *S. cerevisiae*. Activation of Hog1 protein enables yeast cells to cope with and survive through high osmolarity environments. Constitutive activation of Hog1 protein through a mutation at the 318th amino acid critically effects the osmotic stress response pathway.

This MSc thesis aims to investigate the mechanism of act of the F318L mutation on the protein Hog1 and its impact on constitutively activation of Hog1. By using several computational chemistry methods, this study will illuminate how this specific amino acid substitution alters Hog1 activation dynamics.

2. MATERIALS AND METHODS

2.1 Molecular Mechanics

Molecular dynamics is a computational technique used to investigate the behavior and dynamics of systems at the atomic level. It provides a detailed understanding of how atoms and molecules move and interact over time. By simulating the motion of particles according to classical mechanics principles, molecular dynamics allows scientists to explore the properties and behavior of complex proteins that would be challenging to study experimentally.

Molecular dynamics simulations generate the system's trajectory by numerically integrating Newton's equations of motion. The system is subjected to an initial force based on its energy, and the resulting atom coordinates are calculated. This process involves evaluating the forces acting on each atom, taking into account interatomic interactions described by a force field or potential energy function. The acceleration of atoms is determined by the forces applied on them, which subsequently affects their velocities.

Once the new velocities of the atoms are obtained, the displacement of each atom is calculated based on its current velocity and a time step. This displacement is then used to update the coordinates of the atoms. By repeating these calculations at certain intervals, the system's behavior can be plotted over time, revealing its dynamic properties and allowing the observation of various physical phenomena.

Molecular dynamics simulations provide valuable insights into a wide range of scientific questions. They can illuminate the folding mechanisms of proteins, the behavior of enzymes, the interactions between drug molecules and receptor. Through the analysis of trajectories generated by molecular dynamics, scientists can obtain important information such as thermodynamic properties, structural changes, reaction mechanisms, and diffusion rates.

2.2 Force Fields

Force fields play a crucial role in molecular simulations by enabling the calculation of system energy and the derivation of forces acting on the atoms. They are composed of a set of parameters and mathematical functions used for these calculations. The parameters within force fields are determined through a combination of experimental data and quantum mechanical calculations. Initially, these parameters are developed and optimized for smaller systems and can then be applied to larger systems through a process known as parameter transferability.

Force fields can be categorized into two main types: bonded interactions and non-bonded interactions. Bonded interactions cover the stretching of chemical bonds, the bending of bond angles, and torsional rotations. These interactions are described by specific mathematical equations that capture the potential energy associated with these bond movements. On the other hand, non-bonded interactions include electrostatic energy and van der Waals interactions. Electrostatic interactions account for the attraction or repulsion of charged particles, while van der Waals interactions describe the attractive forces between neutral atoms or molecules due to temporary fluctuations in electron distributions.

General equation of a force field includes the below terms in equation 2.1:

$$E = E_{bond}+E_{angle}+E_{dihedrals}+E_{non\text{-}bonded}$$

$$E = \sum_{bonds} k_B(b_i-b_0)^2 + \sum_{angles} k_\theta(\theta_i-\theta_0)^2 + \sum_{dihedrals} 1/2V_n(1+\cos(n_{\phi-\delta}))^2 + \sum_{i-j} (A_{ij}/(r_{ij})^{12}) - (B_{ij}/(r_{ij})^6 + (q_iq_j/r_{ij}) \quad (2.1)$$

2.2.1 Bond stretching

Hooke's Law is applied to determine the energy associated with the deviation from the reference bond length in force field calculations. The reference bond length represents the equilibrium length at which all other terms in the force field have a neutral effect, meaning they do not contribute to the energy. Bond streching term contributing the total energy can be expressed as below:

$$E_{bonds} = \sum k_B(b_i-b_0)^2 \quad (2.2)$$

In the equation 2.2, k_B is the force constant, b_i is the bond length at any moment and b_0 is the reference.

2.2.2 Angle bending

Energy change results from the angle change between three atoms is also calculated by utilizing the Hooke's Law. Equation for angle bending can be found below:

$$E_{angle} = \sum k_{\theta}(\theta_i-\theta_0)^2 \quad (2.3)$$

In the equation 2.3, k_{θ} is the force constant, θ_i is the angle of atoms at any point and θ_0 is the reference value of the angle.

2.2.3 Dihedrals

In force fields, dihedral potentials are included to account for the dihedral angles, which cannot be expressed in other terms. A dihedral angle is formed by four consecutive atoms, representing the angle between two planes formed by the first, second, and third atoms, and the second, third, and fourth atoms. The rotations of these bonds play a crucial role in molecular dynamics simulations as they greatly influence the conformational behavior of molecules. By incorporating dihedral potentials into the force field calculations, the impact of these bond rotations on the overall energy and behavior of the system can be properly accounted for.

$$E_{dihedrals} = \sum (1/2)V_n(1+\cos(n\phi-\delta))^2 \quad (2.4)$$

In equation 2.4, V_n is rotational barrier height, ϕ is dihedral angle at any given time, n is the number of minima and δ is used to adjust the positions of the minima and maxima on the rotational potential energy surface.

2.2.4 Non-bonded interactions

There are two categories of non-bonded interactions: electrostatic interactions and van der Waals interactions.

Electrostatic interactions arise from the unequal charge distribution between atoms, as atoms have different electronegativities. In force fields, static point charges are assigned to atoms within molecules to accurately represent their charge distribution. These point charges enable the calculation of electrostatic interactions between them, employing Coulomb's Law.

Furthermore, van der Waals interactions constitute another type of non-bonded interaction. The calculation of van der Waals interactions is accomplished using the

Lennard-Jones potential, which takes into account the attractive forces between atoms and the repulsive forces arising from their overlapping electron clouds.

1-2 and 1-3 atom interactions are not included in the non-bonded energy calculations since these interactions are already included in the bond stretching and angle bending terms. Equation belonging ton on-bonded interaction energy calculations are given in equation 2.5.

$$E_{non\text{-}bonded} = \sum_{i\text{-}j} (A_{ij}/(r_{ij})^{12}) - (B_{ij}/(r_{ij})^{6} + (q_i q_j/r_{ij}) \quad (2.5)$$

2.3 Molecular Dynamic Simulations

Simulations were run using Amber 16 molecular dynamic package. Topology files were prepared in tleap program using FF14SB force field, JC monovalent ion parameters, LRCM divalent ion parameters and TIP3P water model.

Initial structure was taken from a homology modeling study performed byAlphaFold protein structure database.

A truncated octahedron periodic water box was selected for explicit solvation of systems. The minimum distance between the 14 edge of the box and the protein was set to be 10Å. Then, counterions (K^+) were added to neutralize the overall charge of the system.

First 500 steps of the minimization was performed using steepest descent method to quickly approach to the local minimum. Then, conjugate gradients methods is applied to provide more precise approach to the local minimum. Convergence criteria was set as root mean square of 0.01 $kcal.mol^{-1}.Å^{-1}$.

For equilibration phase, system was firstly heated from 10K to 303K. Systems were heated using Langevin thermostat with 5 ps^{-1} collision frequency. SHAKE algorithm was applied for freezing heavy atom-H atom stretching and time step was set to 2 fs. Simulations were run on periodic boundary conditions. Particle mesh ewald was used for calculating long-range electrostatic interactions and 9Å cut off was selected. The equilibration was carried out in NPT ensemble. The initial velocities of systems were randomly assigned in accordance with Boltzmann distribution. For production phase, systems were run in 303 K in NPT ensemble.

3. RESULTS

3.1 Alphafold Structure as the Initial Geometry

Yeast Hog1 protein does not have a crystal structure, thus we have used a predicted model of the Hog1 protein from AlphaFold Protein Structure Database (Figure 3.1).

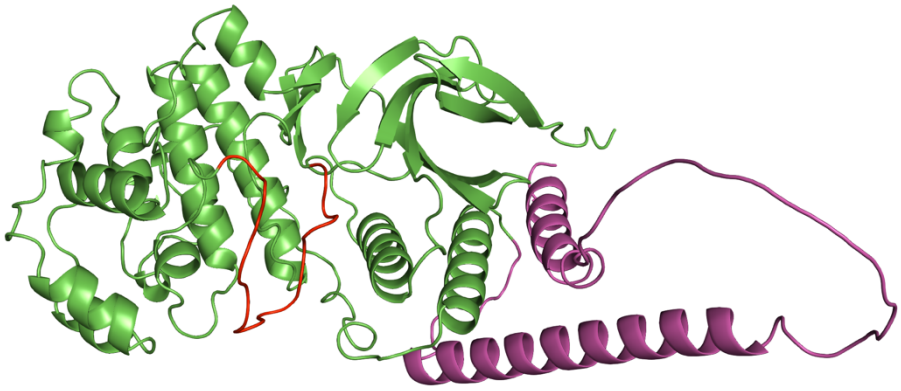

Figure 3.1: AlphaFold predicted structure of yeast Hog1 protein. Green regions are the regions that are found both in yeast Hog1 and human analogue of Hog1 protein. Phosphorylation loop, which is also found both in yeast Hog1 and its human analogue is shown in red. Pink is the region that is found in the yeast Hog1 but not in the human analogue of it.

Hog1 predicted structure is taken from AlphaFold Protein Structure Database and aligned with crystal structures of a human MAPK protein called Erk2, 1ERK and 2ERK crystal pdb files. 1ERK is non-phosphorylated form of the protein, whereas 2ERK is the phosphorylated form (Figure 3.2).

It is clearly visible from the alignement in Figure 3.2 that AlphaFold software is succesful in creating an initial structure to use in Molecular Dynamics simulations. Compared with the crystal structures, conserved regions are predicted as having the same tertiary structures using AlphaFold. Erk2 lacks a 77 amino acid region at the C terminal region of the protein with respect to Hog1, thus 1ERK and 2ERK crystals are missing the alpha-helix and unstructured region that can be seen in Figure 3.1 as pink region.

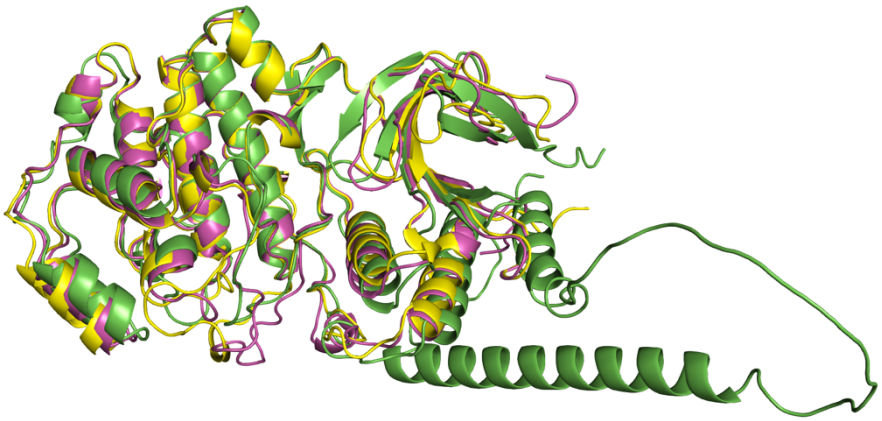

Figure 3.2: Alignment of Hog1 AlphaFold predicted (green), 1ERK (yellow) and 2ERK (pink) pdb files.

3.2 Important Interactions in the Alphafold Structure and Preparation of Initial Geometries

The phosphorylation lip, ATP binding site and a hydrophobic cluster including the site of mutation (F318/L318) are the main focus of this study because these sites are affected by mutation, nucleotide binding and phosphorylation. Figure 3.3 shows the positions of the important residues in the phosphorylation lip and active site in the Alphafold structure. The active site in the absence of ATP and substrate is indicated by the red circle. Y176, one of the residues that will be phosphorylated closes he entrance of the active site. The other target of phosphorylation, T174 is oriented away from the active site. The positions of T174 and Y176 are similar to their counterparts in unphosphorylated Erk2 and p38 crystals (PDB codes: 1erk and 1wfc). Thus, the conformation of the lip is a closed conformation found in unphosphorylated MAP kinases in the literature. L165, which is thought to guide the substrate, is situated next to the ATP binding site marked by N149 and D162. T174 and Y176 are surrounded by six arginine residues that have the potential of interacting with these two amino acids when they are phosphorylated**.**

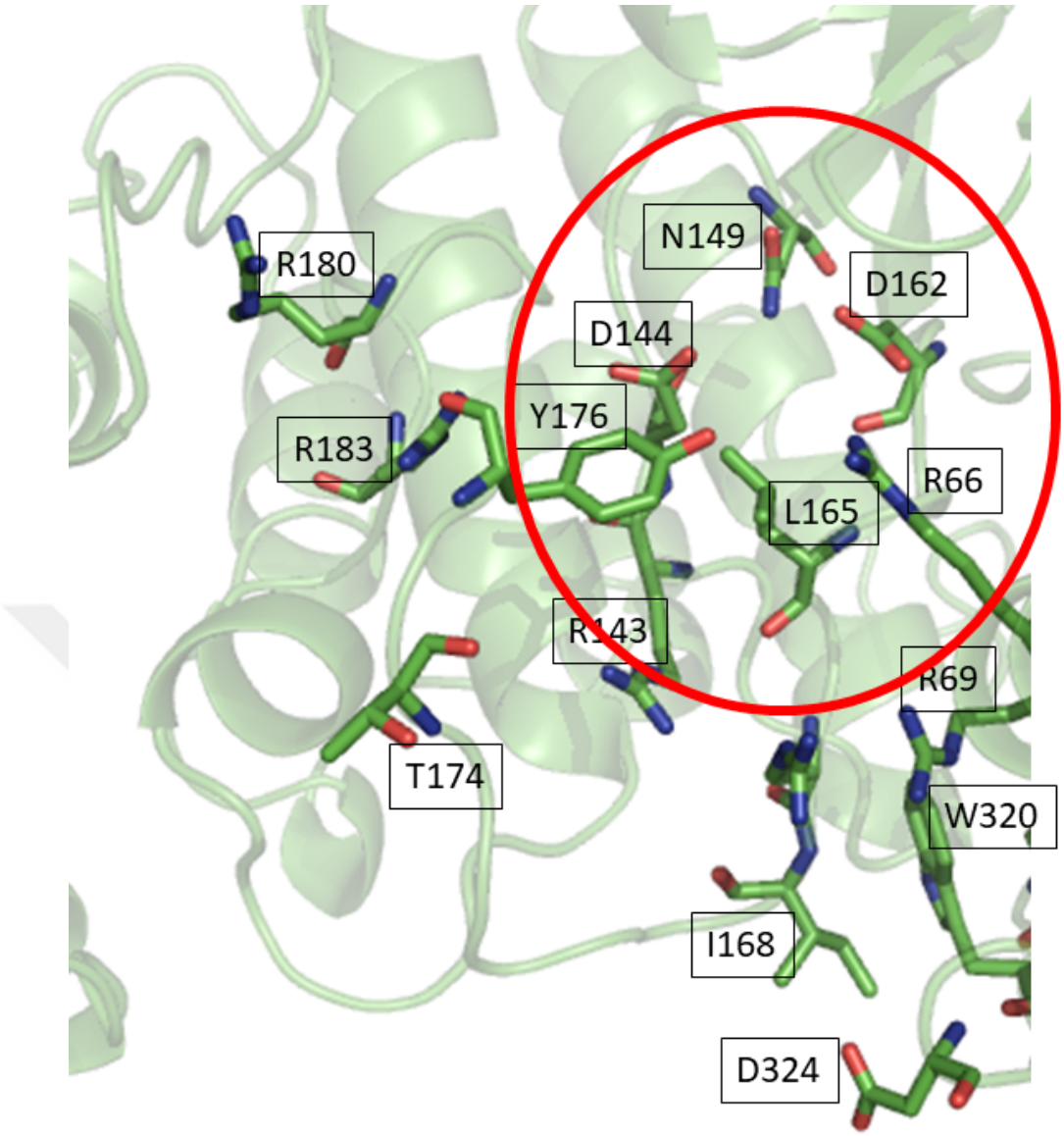

Figure 3.3: T174 and Y176 amino acids and their interaction partners around the phosphorylation loop.

The initial geometries of the ATP bound structures (Figure 3.4) have been prepared by aligning the Alphafold structure to the cAMP-dependent protein kinase (PDB code: 1atp) where a bound ATP can be seen. In the structure we have pepared, the adenine moiety forms hydrogen bonds to to the backbone of E101 and Q103. L151 forms a hydrophobic contact with adenine. D106 makes a hyrogen bond with the 3' oxygen atom of the ribose ring. N149 and D162 are complexed with the two Mg^{2+} ions that coordinate ATP. E70 interacts with Mg^{2+} in a water mediated way.

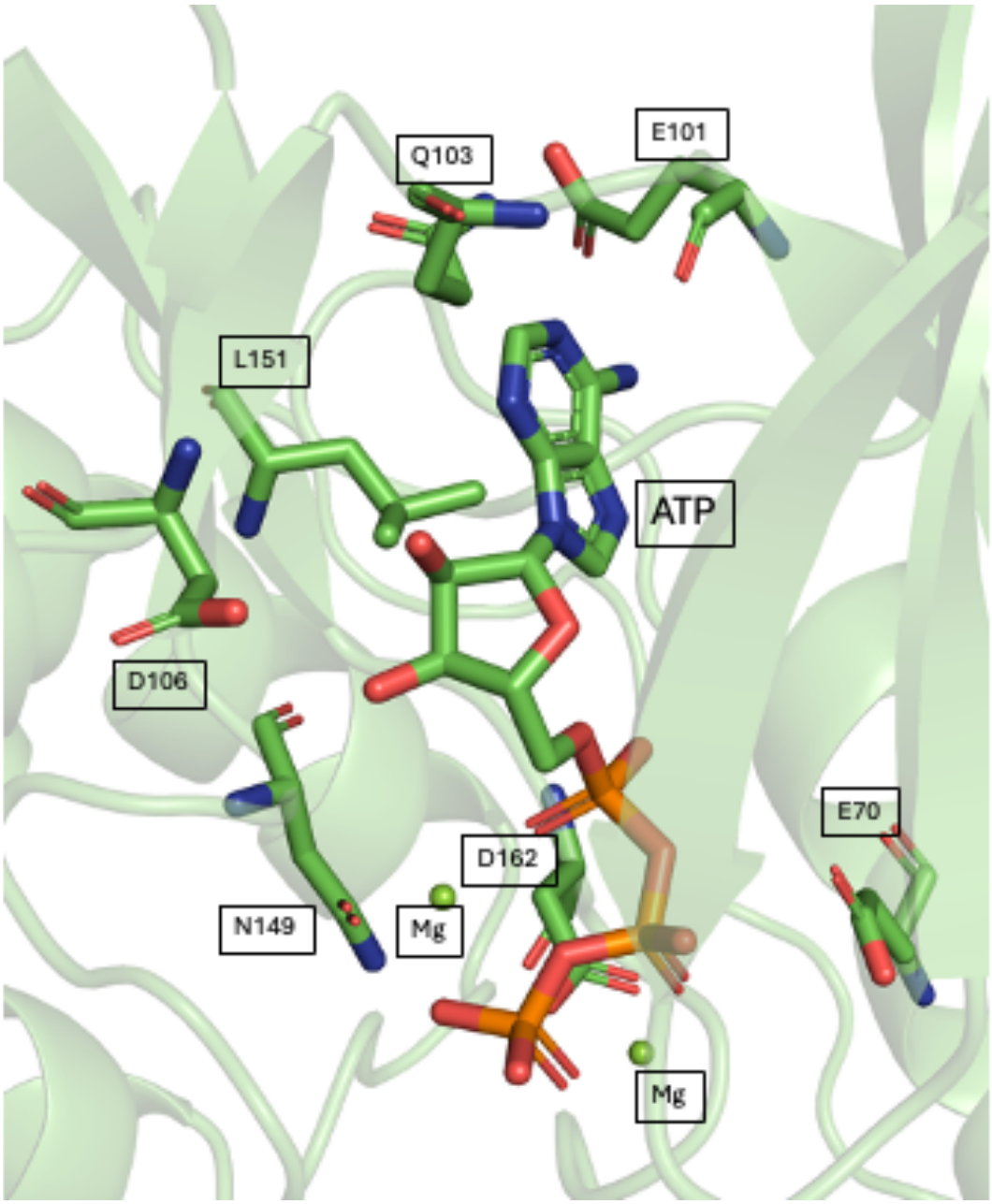

Figure 3.4: Position of ATP and its interaction partners in HOG1 model.

The residue subject to mutation, F318, resides in a hydrophobic cluster made of W320, F322, L73, F359, W332 and Y68 (Figure 3.4). In addition, L165 and I168 are also potential interaction partners of this hydropobic cluster. As shown in the next sections, either one of these residues move during simulations to interact with the hydrophobic cluster.

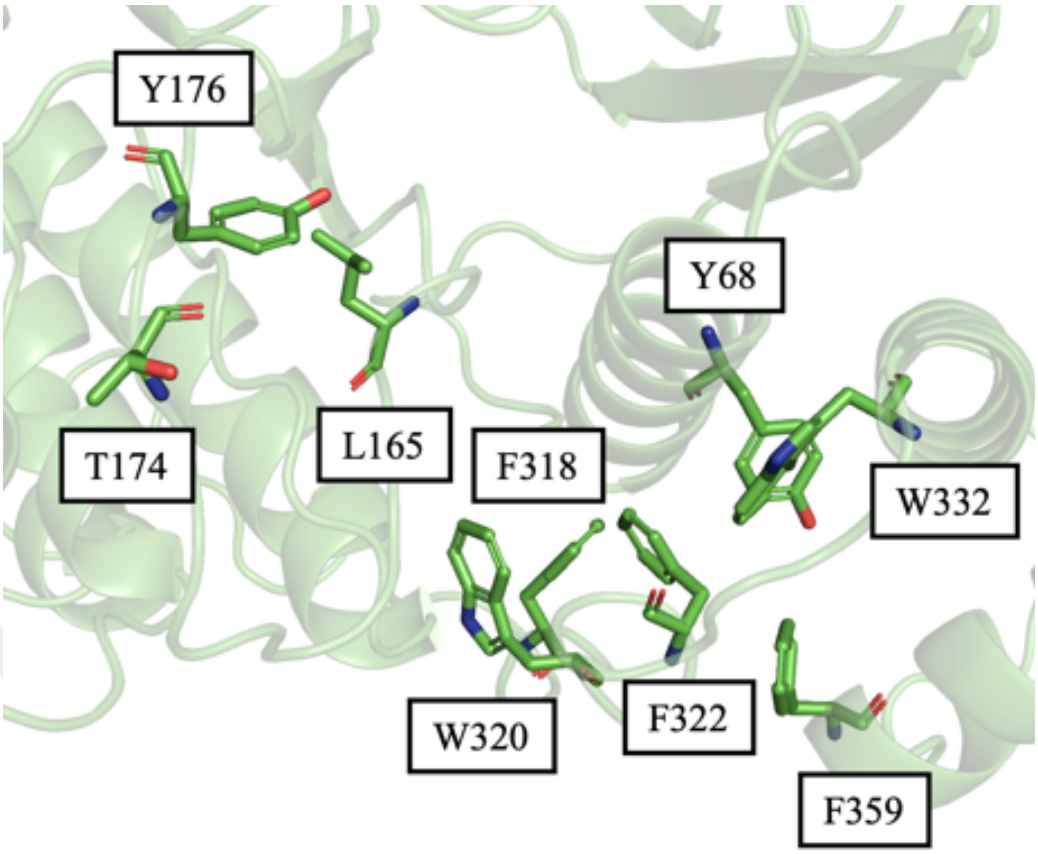

Figure 3.5: Aromatic cluster around the mutation zone and surrounding interaction partners.

Since the mutation involves the hydrophobic cluster, it is important to unambiguously determine the organization at this region. Hence, for each of the wild type and mutant systems, alternative initial geometries have been prepared by either changing the orientation of W320 or F322 (Figure 3.5). W320 side chain has been rotated away from the hydrophobic cluster into the solvent. F322 side chain has been reoriented toward F359.

Mutant initial geometries have been designed by manually changing F318 to leucine. For each of the three arrangement of the hydrophobic cluster described above, mutant structures have been prepared.

Phosphorylated systems have been obtained by manually adding phosphate groups to both T174 and Y176 in the Alphafold structure. Since mutants are constitutively active even without phosphorylation, only wild type proteins have been subjected to phosphorylation in this study.

In addition, at the end of 1 μs simulation in a wild type, nucleotide-free, unphosphorylated system, phosphate groups have been added and simulated for one

more μs. Conversely, at the end of 1 μs simulation in a wild type, nucleotide-free, phosphorylated system, phosphate groups have been removed and simulated for one more μs. Finally, a mutant, nucleotide-free, unphosphorylated system has been converted to wild type at the end of 1 μs and simulated for another μs.

Table 3.1 summarizes the properties of the initial geometries, their nomenclature and simulation durations.

Table 3.1: Nomenclature, properties and simulation durations of alternative system.

Simulation Name	Initial Structure	Simulation Duration
WT	Alphafold Hog1 structure prediction	3 μs
WTATP	WT in ATP bound form	12 μs
WTPP	Nucleotide-free, dual phosphorylated WT	1 μs
WTATPPP	Dual phosphorylated and ATP bound WT	9 μs
WTATPY	WT in ATP bound form, W320 side chain manually turned into solvent	10.6 μs
WTATPYY	WT in ATP bound form, F322 side chain turned towards F359 instead of F318	4 μs
WTATPPPY	Dual phosphorylated and ATP bound WT, W320 side chain manually turned into solvent	9.4 μs
WTPPSIL	Unphosphorylated nucleotide-free WT, prepared by removing phosphates after 1 μs in a simulation on the phosphorylated system	1 μs

Table 3.1 (continued): Nomenclature, properties and simulation durations of alternative system.

Simulation Name	Initial Structure	Simulation Duration
WTPPEKLE	Dual phosphorylated nucleotide-free WT, prepared by adding phosphates after 1 μs in a simulation on the unphosphorylated system	1 μs
WTMUTTAN	WT HOG1 model, obtained by manually manipulating a structure from a mutant simulation	1 μs
MUT	Alphafold HOG1 prediction, F318 manually changed to leucine residue	4 μs
MUTATP	MUT in ATP bound form	13 μs
MUTATPY	MUT in ATP bound form, W320 side chain manually turned into solvent	7.9 μs
MUTATPYY	MUT in ATP bound form, F322 side chain turned towards F359 instead of F318	3.8 μs

3.3 Wild type, Unphosphorylated, Nucleotide-free Simulations

The rmsd plots of the three wild type, unphosphorylated, nucleotide-free simulations are displayed in Figures 3.6, 3.8, and 3.9. The rmsd values of the lip comprising residues 161-179 are also given in these figures.

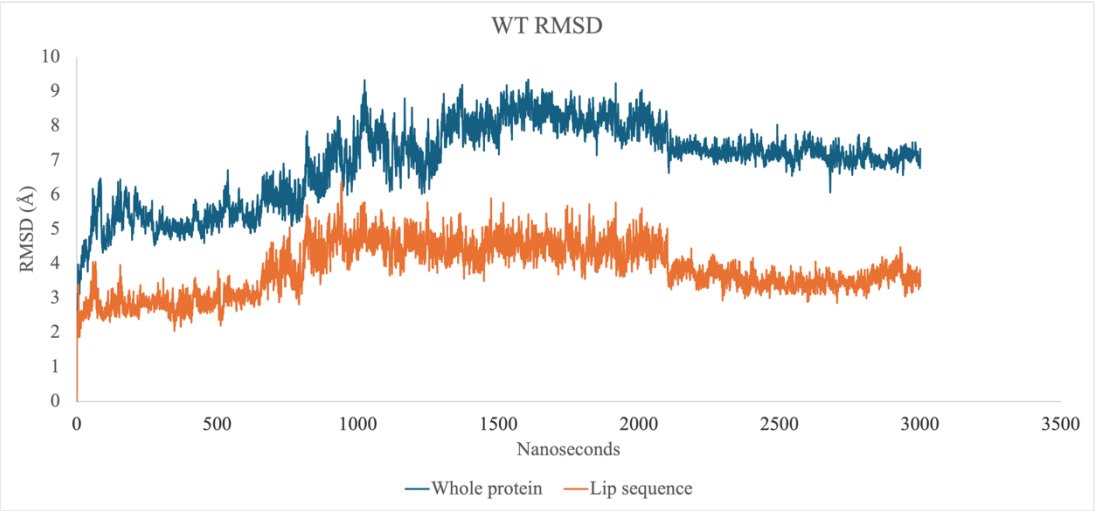

Figure 3.6: RMSD graph of whole protein (blue) and RMSD graph of lip sequence (orange) in WT model.

From Figure 3.6, it can be seen that both the overall protein movement and lip movement are equilibrated after 2 μs. When the final geometry is aligned with the Alphafold geometry, an rmsd of 7.295 Å is obtained. If the C-terminal 91 residues that are found only in Hog1, therefore cannot be modelled well by Alphafold are excluded, the rmsd values is reduced to 2.038 Å. Thus, the regions common to all MAP kinases are well modelled by Alphafold and the deviation from the initial structre is small. The alignment of the final structure in the simulation and the Alphafold structure is given in Figure 3.7 A.

The position of the lip at the end of the simulation can be seen in Figure 3.7 B. Like in the unphosphorylated Erk2, it closes the active site, Y176 being situated between D144 and R143. Leu165 flanks the actve site indicated by the red circle in Figure 3.7 B.

In the final geometry, unlike the initial structure, W320 is oriented into the solvent. Its initial position is now occupied by I168. As a result, I168 makes hydrophobic interactions with L73, F318 and F322. The region that contains I355 is unstructured in the initial Alphafold structure. However, this region acquires a helical geometry during the simulation and I355 makes hydrophobic interactions with F318, thus becomes part of the hydrophobic cluster.

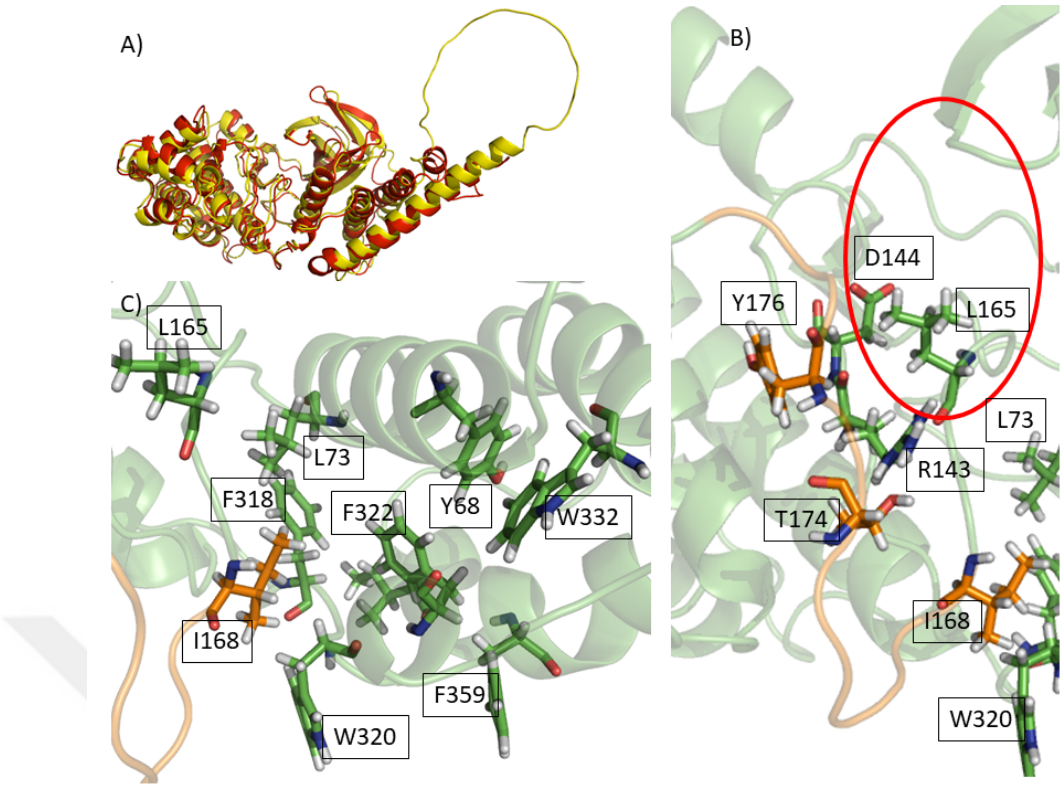

Figure 3.7: Alignment of Alphafold predicted structure of Hog1 protein and snapshot taken from WT model (A), close-up snapshot taken from phosphorylation lip in WT model with important residues as sticks and active site is denoted by a red circle (B), and close-up snapshot taken from hydrophobic cluster in WT model with important residues as sticks (C).

The rmsd plots of the other unphosphorylated, nucleotide-free, wild type simulations, WTPPSIL and WTMUTTAN, are given in Figures 3.8 and 3.9. These figures show that WTPPSIL is stable during 1 microsecond simulation time whereas WTTMUTTAN becomes equilibrated after 700 ns.

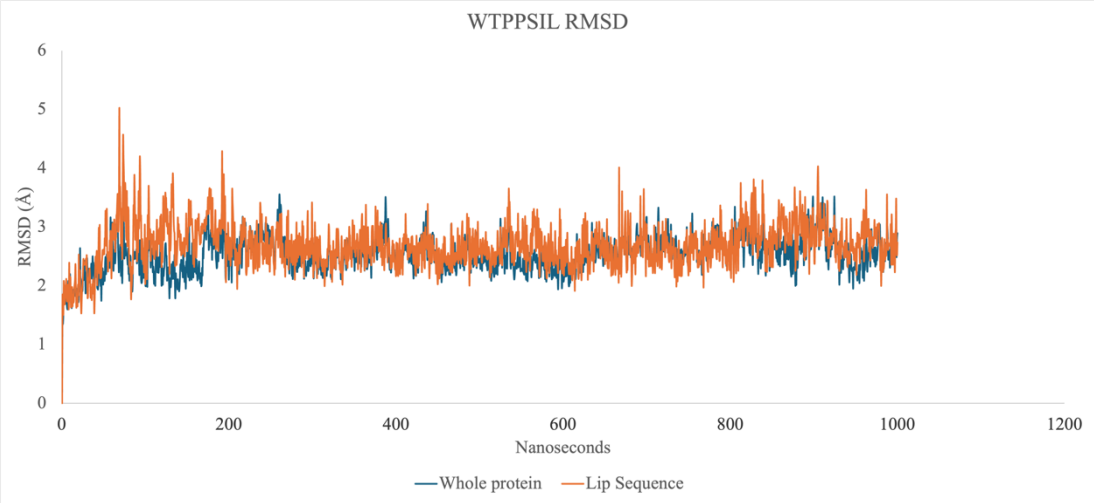

Figure 3.8: RMSD graph of whole protein (blue) and RMSD graph of lip sequence (orange) in WTPPSIL model.

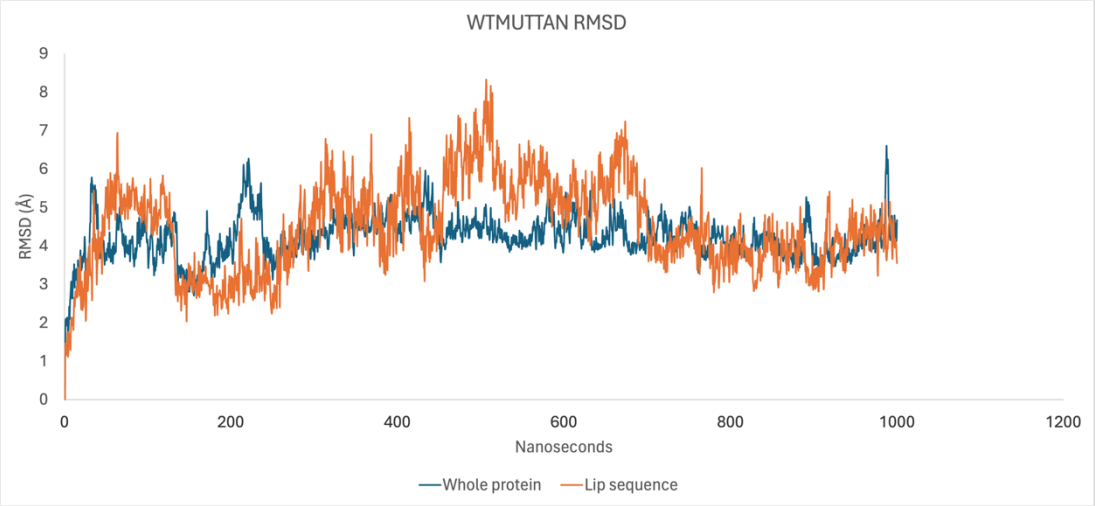

Figure 3.9: RMSD graph of whole protein (blue) and RMSD graph of lip sequence (orange) in WTMUTTAN model.

3.4 Wild type, Dual Phosphorylated, Nucleotide-free Simulations

Two dual phosphorylated, nucleotide-free wild type models' rmsd plots are given in Figures 3.10 and 3.12. Rmsd plots belonging to lip sequences of these two models are also given in the same figures.

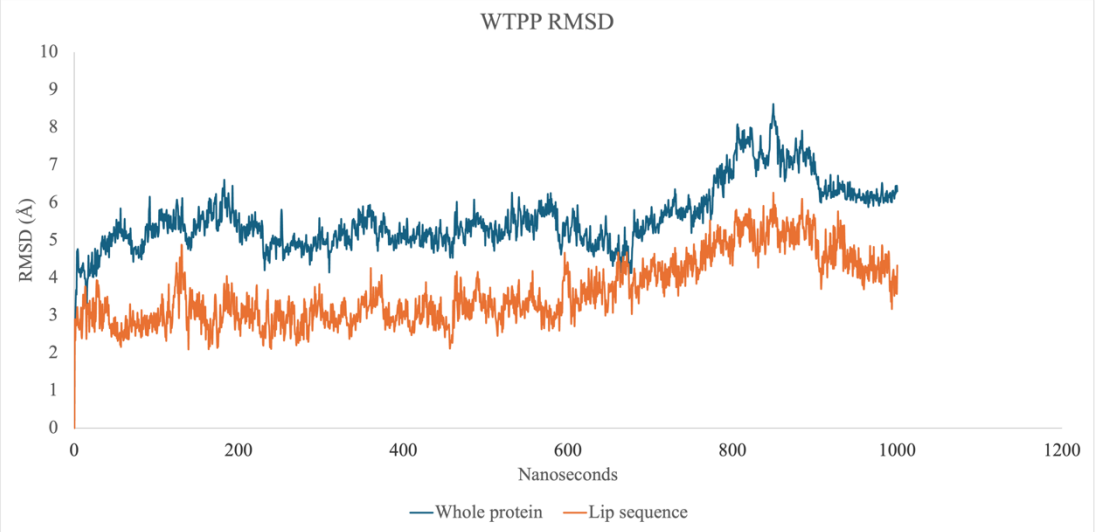

Figure 3.10: RMSD graph of whole protein (blue) and RMSD graph of lip sequence (orange) in WTPP model.

In Figure 3.10, we can see conformational changes in the protein conformation. Lip conformation also shows a change at the same time point of the simulation.

When the initial and final geometries of WTPP model are aligned, an rmsd of 6.274 Å is obtained. When C-terminal 91 residues are excluded in the rmsd calculations, rmsd value is reduced to 1.674 Å. This shows that majority of the conformational changes

are occurring in the C-terminal unstructured region of the protein. Aligned initial and final geometries of WTPP model are given in Figure 3.11 A.

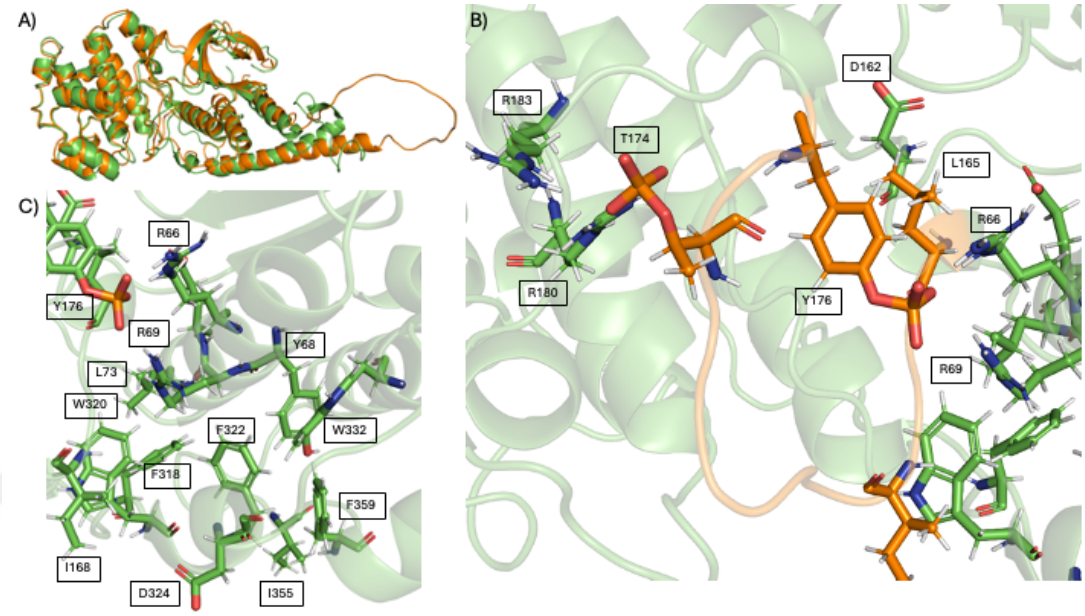

Figure 3.11: Alignment of initial and final geometries of WTPP model (A), close-up snapshot taken from phosphorylation lip in WTPP model with important residues as sticks (B), and close-up snapshot taken from hydrophobic cluster in WTPP model with important residues as sticks (C).

In Figure 3.11 B, Phosphorylated T174 is interacting with two arginine residues R180 and R183 through its phosphate oxygens. Phosphorylated Y176 is forming salt bridge interactions with R66 and R69.

In Figure 3.11 C, hydrophobic cluster of WTPP model is seen. L165 is facing away from the hydrophobic cluster and positioned itself in the active site as in the WT model. I168 is interacting with W320.

In Figure 3.12, conformational changes are observed both in overall protein and lip sequence.

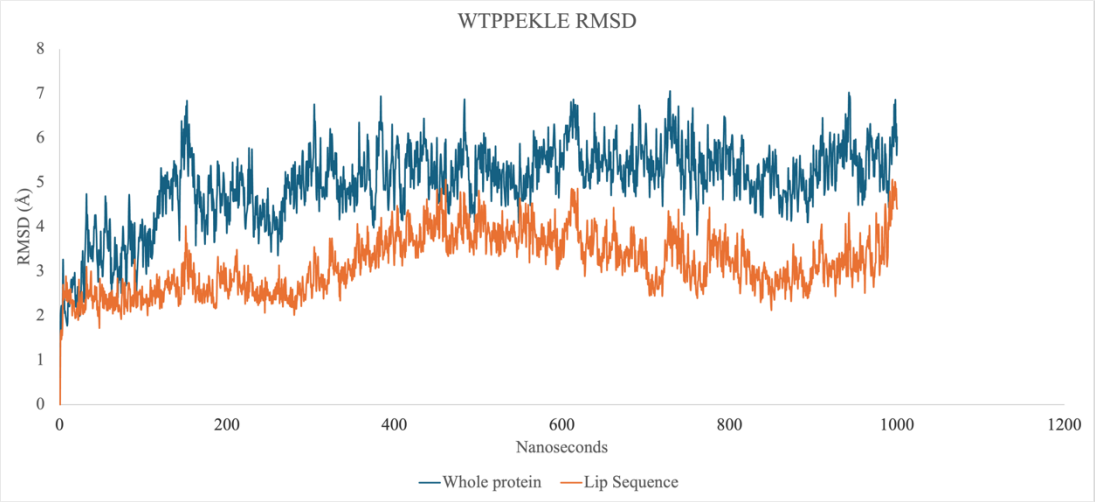

Figure 3.12: RMSD graph of whole protein (blue) and RMSD graph of lip sequence (orange) in WTPPEKLE model.

When the initial and final geometries of WTPPEKLE model are aligned, an rmsd of 5.982 Å is obtained. When C-terminal 91 residues are excluded in the rmsd calculations, rmsd value is reduced to 2.152 Å. This shows that majority of the conformational changes are occurring in the C-terminal unstructured region of the protein. Aligned initial and final geometries of WTPPEKLE model are given in Figure 3.13 A.

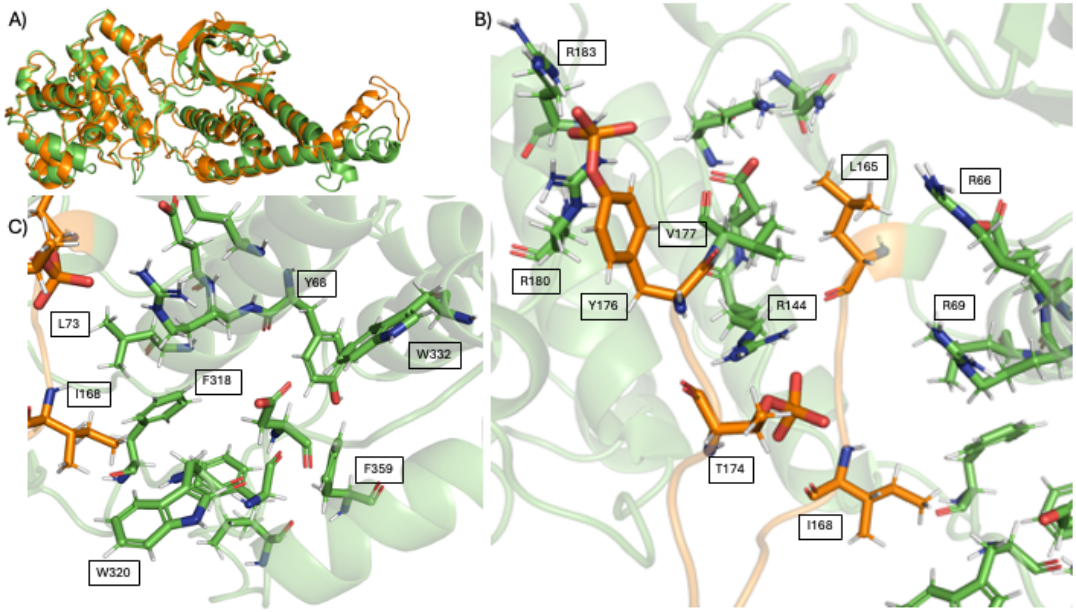

Figure 3.13: Alignment of initial and final geometries of WTPPEKLE model (A), close-up snapshot taken from phosphorylation lip in WTPPEKLE model with important residues as sticks (B), and close-up snapshot taken from hydrophobic cluster in WTPPEKLE model with important residues as sticks (C).

Phosphorylation lip of WTPPEKLE model can be seen in Figure 3.13 B. L165 is occupying the active site, interacting with V177. Phosphorylated Y176 is making salt bridge interactions with R180 and R183 through its phosphate group. Unlike in the WTPP model, phosphorylated T174 is not interacting with R66 and R69 residues. However, simulation time might not be enough to form these interactions and extended simulations would show the interaction.

In Figure 3.13 C, I168 is interacting with W320 and F318, thus became a part of the hydrophobic cluster. F318 is also interacting with L73. W332 is interacting with Y68. Also, W320 turns its side chain towards the solvent.

3.5 Wild type, Unphosphorylated, ATP Bound Simulations

Rmsd plots of whole protein belonging to three unphosphorylated, ATP bound simulations are given in igures 3.14, 3.16, and 3.18. Rmsd plots of lip sequences of these three models are also given in the same figures.

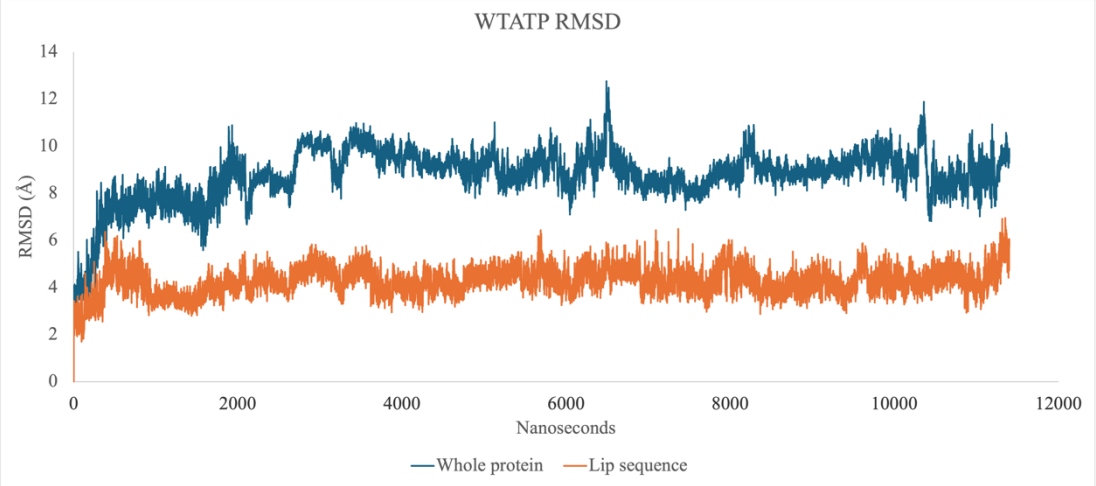

Figure 3.14: RMSD graph of whole protein (blue) and RMSD graph of lip sequence (orange) in WTATP model.

From Figure 3.14, we can see two changes in the protein conformation. Lip conformation also shows a change in the last parts of the simulation.

When the initial and final geometries of WTATP model are aligned, an rmsd of 9.488 Å is obtained. When C-terminal 91 residues are excluded in the rmsd calculations, rmsd value is reduced to 3.615 Å. This shows that majority of the conformational changes are occurring in the C-terminal unstructured region of the protein. Aligned initial and final geometries of WTATP model are given in Figure 3.15 A.

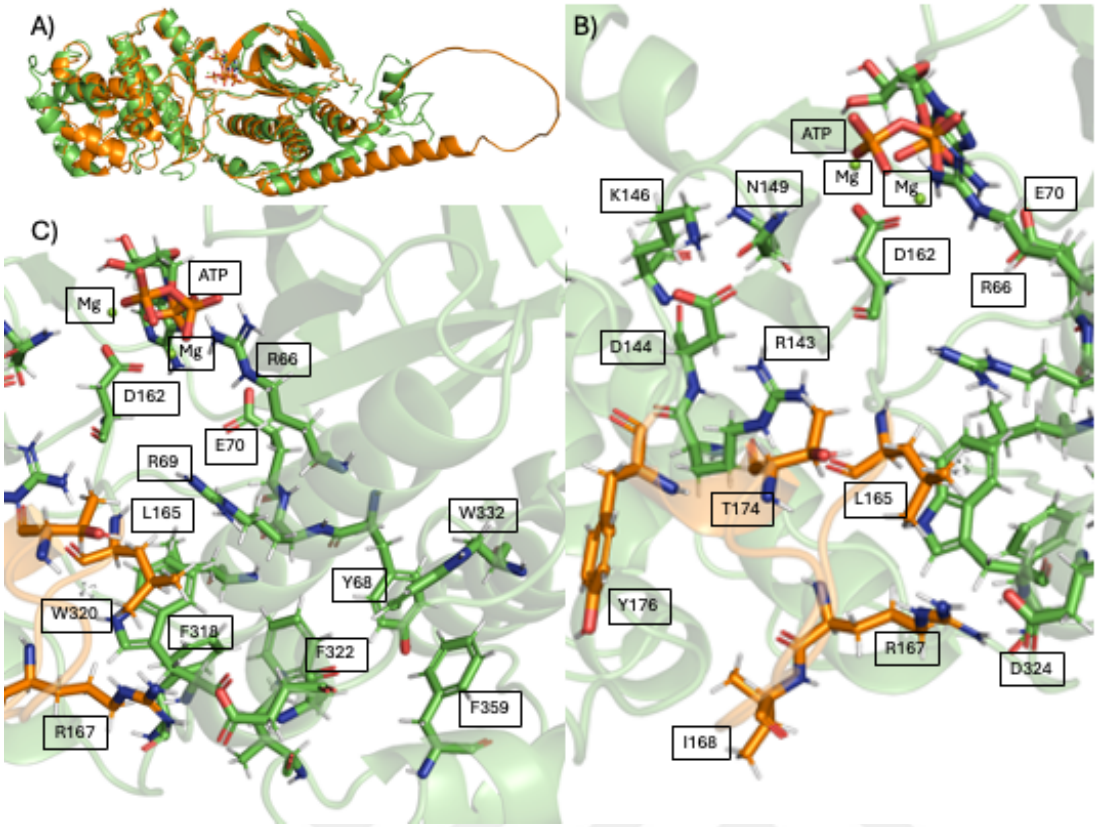

Figure 3.15: Alignment of initial and final geometries of WTATP model (A), close-up snapshot taken from phosphorylation lip in WTATP model with important residues as sticks (B), and close-up snapshot taken from hydrophobic cluster in WTATP model with important residues as sticks (C).

The position of the lip at the end of the simulation can be seen in Figure 3.15 B. Lip positioned itself away from the active site and leaves the active site open. L165 blocking the active site in WT model changed its position to allow open active site conformation. R167 is able to interact with D324 due to open lip conformation. I168 is facing towards solvent and is not blocking the L165 as in WT model. However, W320 is blocking the direct interaction of L165 and F318 by positioning itself between these two residues. E70 is coordinating the Mg^{2+} ion through water mediated interactions. D162 is directly involved in the coordination shell of Mg^{2+} ion.

Hydrophobic cluster in the WTATP model is given in Figure 3.15 C. L165 is positioned towards the hydrophobic cluster and interacting with W320, thus became a part of hydrophobic cluster. This positioning of L165 also brings an open position of active site. Hydrophobic cluster reaches a similar geometry in WTATPY and WTATPYY models as shown in Figure 3.11 C. W320 and F322 are turned towards their original positions even though simulations were started as they were facing towards the solvent in WTATPY and WTATPYY models respectively.

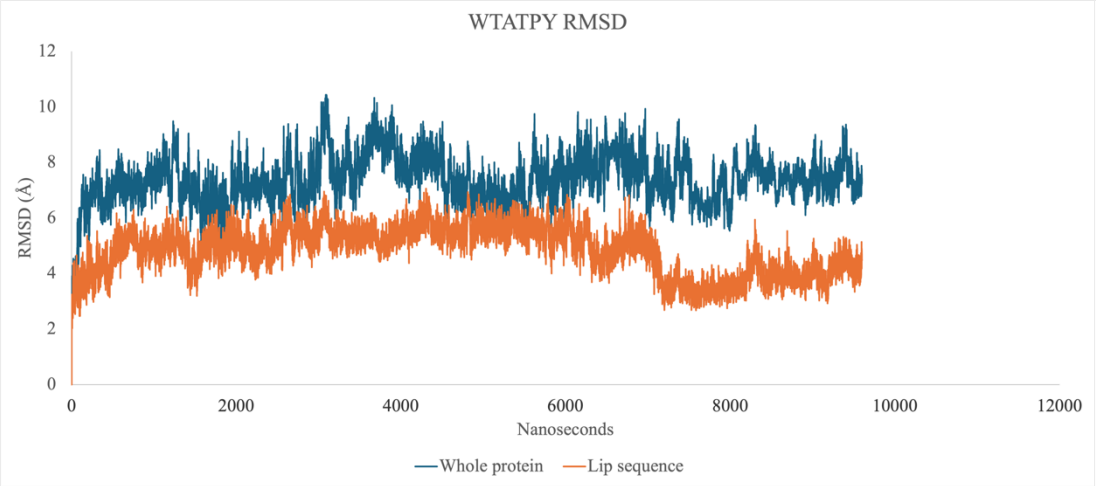

Figure 3.16: RMSD graph of whole protein (blue) and RMSD graph of lip sequence (orange) in WTATPY model.

Figure 3.16 shows us rmsd plots of WTATPY model, both whole protein and lip sequence. Lip sequence shows a conformation change after 1 μs, which is consistent with the changes in rmsd graph of whole protein. When initial and final geometries of WTATPY model aligned, rmsd value of 8.354 Å is obtained. After excluding C-terminal 91 residues, rmsd value is reduced to 2.601 Å. Alignment of initial and final geometries for WTATPY model is given in Figure 3.17 A.

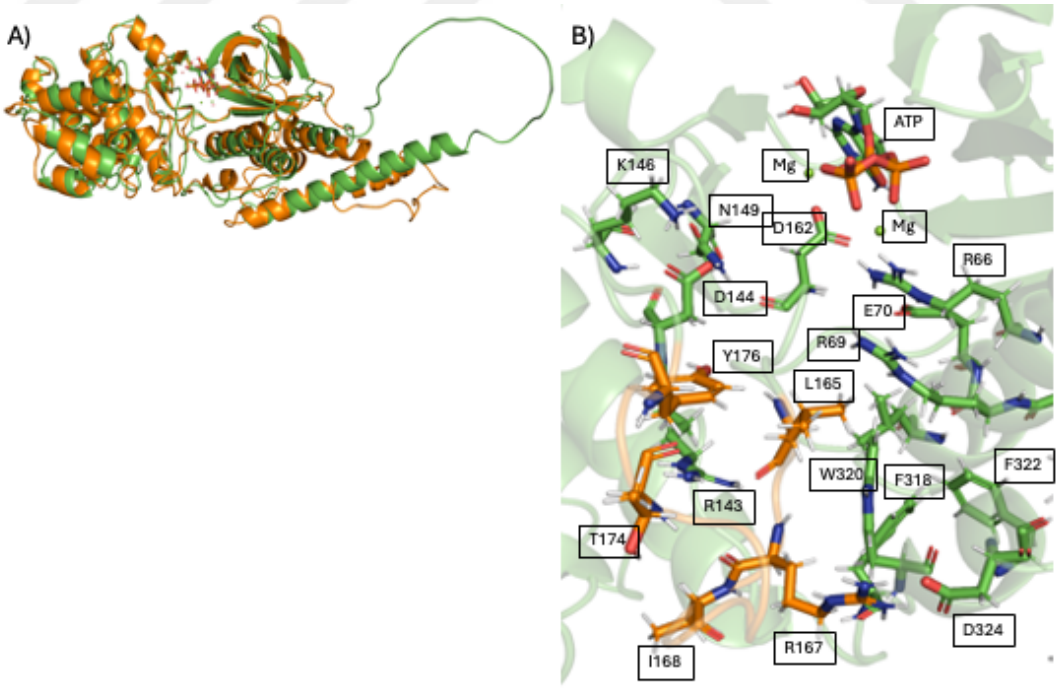

Figure 3.17: Alignment of initial and final geometries of WTATPY model (A) and close-up snapshot taken from phosphorylation lip in WTATPY model with important residues as sticks (B).

In the final geometry shown in Figure 3.17 B, Mg^{2+} ions are coordinated directly by D162. E70 coordinates Mg^{2+} through water mediated interactions. L165 is positioned close to hydrophobic cluster, thus leaves the active site open. Although manually turned towards the solvent in the beginning of the simulation, W320 positioned itself back into hydrophobic cluster and like in WTATP model, interacts with L165, thus blocks the interaction of L165 with F318. R167 interacts with D324 and stabilizes lip in a conformation that opens the active site. Y176 positiones itself in between R143 and D144. F322 is interacting with Y68. T174 is turned towards solvent and away from the active site. F318 is interacting with L73.

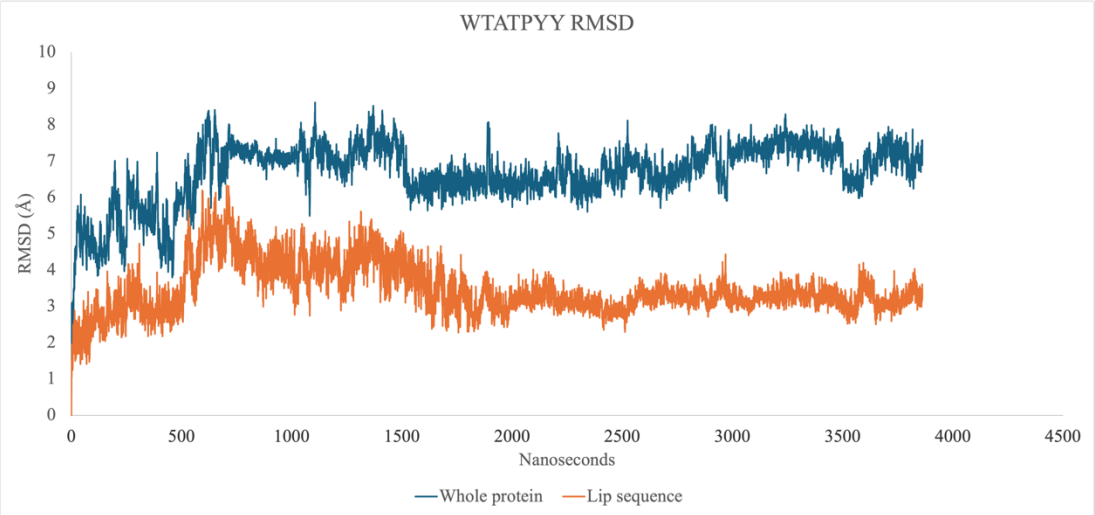

Figure 3.18: RMSD graph of whole protein (blue) and RMSD graph of lip sequence (orange) in WTATPYY model.

Figure 3.18 shows us rmsd plots of WTATPYY model, both whole protein and lip sequence. We can see a conformational change in the protein after 3.5 μs, which simultaneously occurs in the lip conformation. When initial and final geometries of WTATPYY model aligned, rmsd value of 7.178 Å is obtained. After excluding C-terminal 91 residues, rmsd value is reduced to 2.787 Å. Alignment of initial and final geometries for WTATPY model is given in Figure 3.19 A.

Final geometry in Figure 3.19 B 9 shows that Mg^{2+} ions are coordinated directly by D162. E70 coordinates Mg^{2+} through water mediated interactions. Active site is relatively closed compared to other two unphosphorylated, ATP bound models, WTATP and WTATPYY, however it is still open enough to allow binding of other molecules. L165 is interacting with V177 and side chain of L165 turned towards the

lip which positions L165 more closely to the active site compared to WTATP and WTATPY, which is a reason why active site is relatively close.

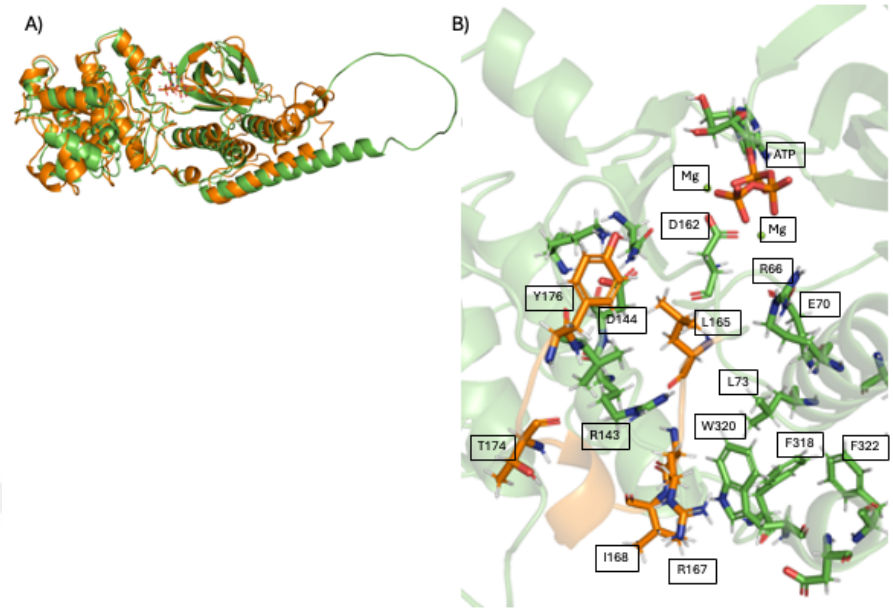

Figure 3.19: Alignment of initial and final geometries of WTATPYY model (A) and close-up snapshot taken from phosphorylation lip in WTATPYY model with important residues as sticks (B).

3.6 Wild type, Dual Phosphorylated, ATP Bound Simulations

Rmsd plots of whole protein belonging to two double phosphorylated, ATP bound simulations are given in Figures 3.20 and 3.22. Rmsd plots of lip sequences of these two models are also given in the same figures.

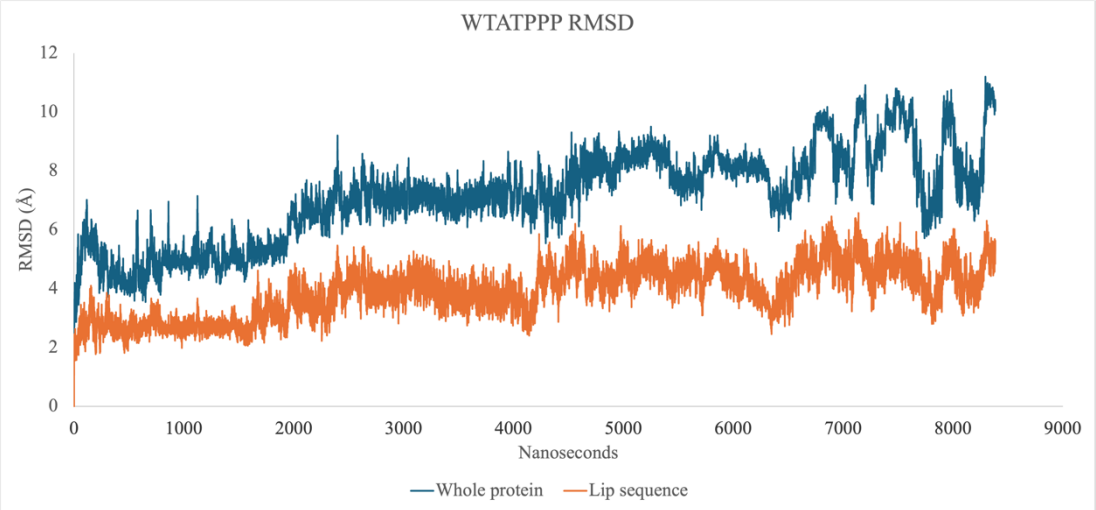

Figure 3.20: RMSD graph of whole protein (blue) and RMSD graph of lip sequence (orange) in WTATPPP model.

Rmsd graphs of WTATPPP model and lip sequence belonging to this model given in Figure 3.16 show conformational changes through the simulation.

When the initial and final geometries of WTATPPP model are aligned, an rmsd of 9.637 Å is obtained. After C-terminal 91 residues are excluded in the rmsd calculations, rmsd value is reduced to 2.808 Å. This shows that majority of the conformational changes are occurring in the c-terminal unstructured region of the protein. Aligned initial and final geometries of WTATPPP model are given in Figure 3.21 A.

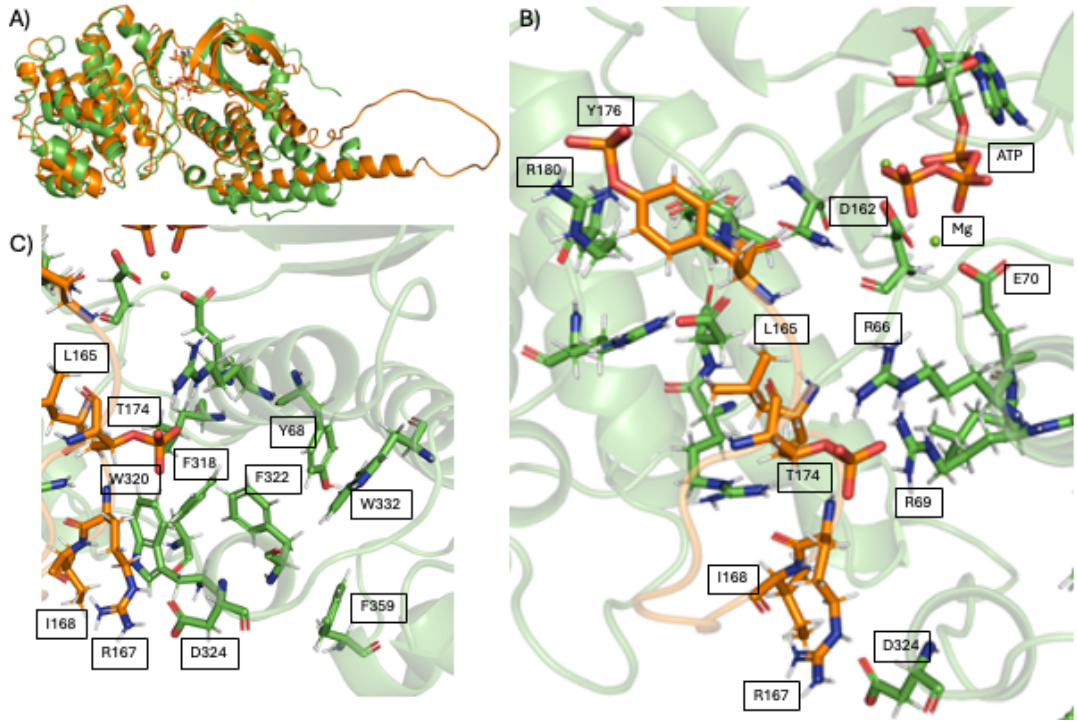

Figure 3.21: Alignment of initial and final geometries of WTATPPP model (A), close-up snapshot taken from phosphorylation lip in WTATPPP model with important residues as sticks (B), and close-up snapshot taken from hydrophobic cluster in WTATPPP model with important residues as sticks (C).

In Figure 3.21 B, phosphorylation lip of WTATPPP model is shown. D162 is directly involved in the coordination shell of Mg^{2+} ion. E70 are involved in the coordination shell of Mg^{2+} via water mediated interactions. Phosphorylated T174 is interacting with R66 and R69 through its phosphate group. Phosphorylated Y176 formed only one salt bridge interactions, with R180, instead of two it is supposed to form, however only one salt bridge is enough to keep the active site open.

Hydrophobic cluster is shown in Figure 3.21 C. Phosphorylated T174 forms a salt bridge interaction with R66, which blocks L165 from entering the hydrophobic cluster. L165 is turned towards the lip, away from F318.

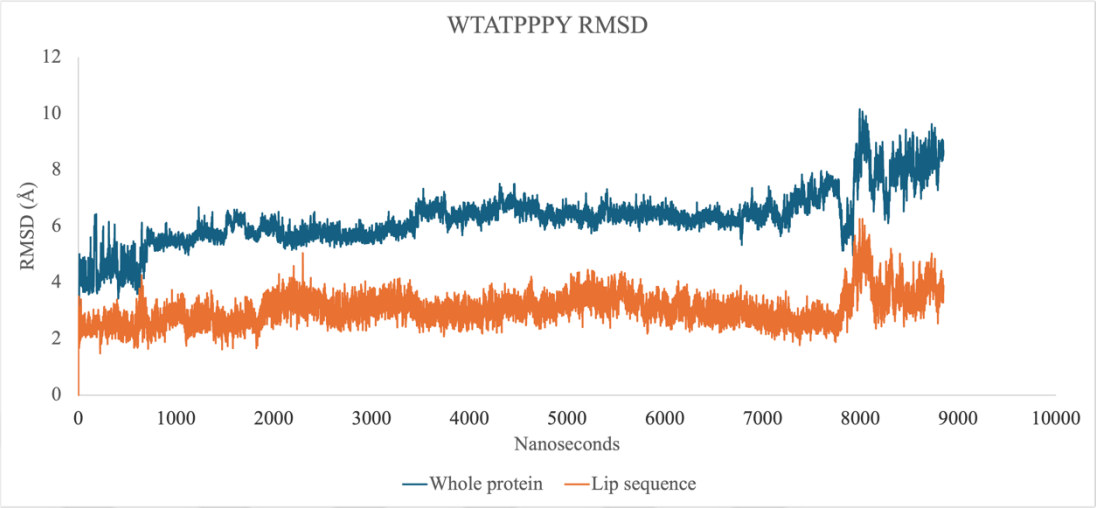

Figure 3.22: RMSD graph of whole protein (blue) and RMSD graph of lip sequence (orange) in WTATPPPY model.

Rmsd graphs of WTATPPPY model and lip sequence belonging to this model given in Figure 3.22 show conformational changes after 8 μs.

When the initial and final geometries of WTATPPPY model are aligned, an rmsd of 8.888 Å is obtained. After C-terminal 91 residues are excluded in the rmsd calculations, rmsd value is reduced to 3.220 Å. This shows that majority of the conformational changes are occurring in the c-terminal unstructured region of the protein. Aligned initial and final geometries of WTATPPPY model are given in Figure 3.23 A.

In final geometry, Figure 3.23 B, T174 and Y176 forms contacts with each other's counterparts as compared to rest of the simulations and crystal structures. Phosphorylated Y176 positioned itself in three arginine residues, R167, R66 and R69, and forms salt bridge interactions through its phosphate group. These salt bridge interactions prevent L165 to get into close proximity of hydrophobic cluster, thus position L165 into the active site. Hence, active site remains closed. Considering the positions of critical residues and the fact that double phosphorylated ATP bound WT protein's active site being open, this final geometry is unlikely to happen, thus this model is not going to be involved in further discussions. Presumably, because of the

strength of the multiple salt bridges, the simulation time was not enough for this geometry to rearrange to the one observed experimentally.

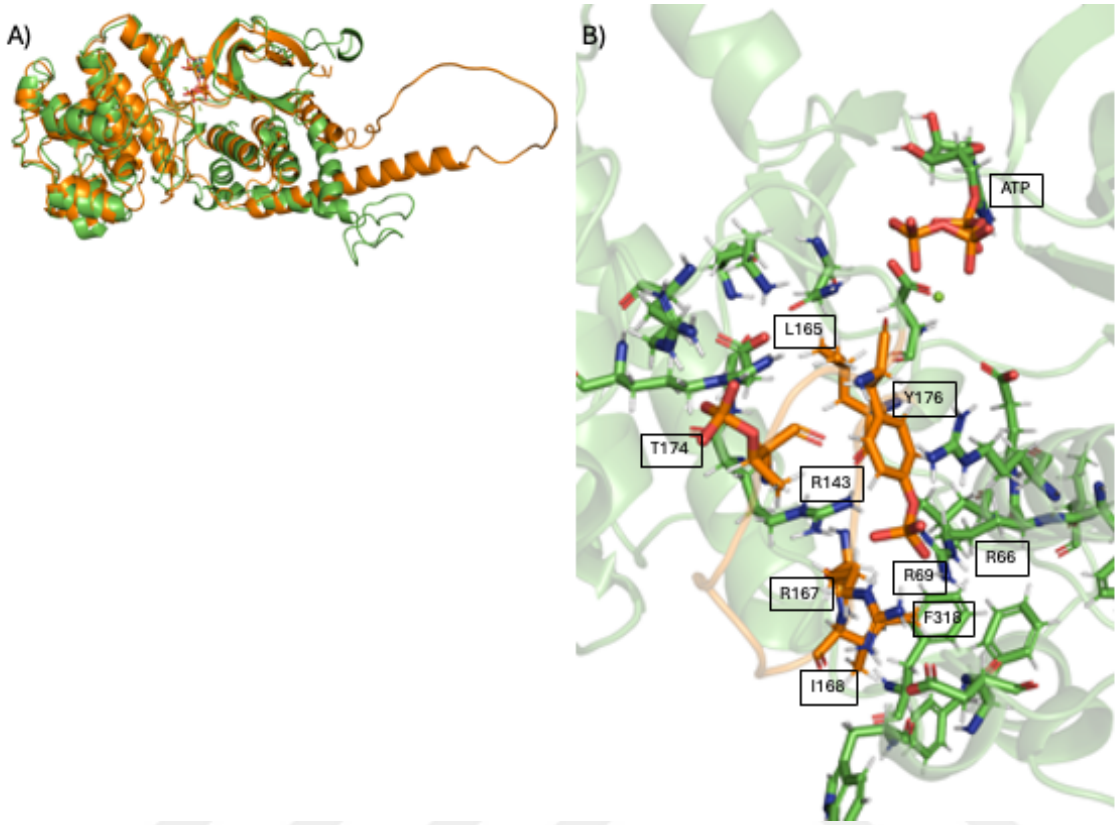

Figure 3.23: Alignment of initial and final geometries of WTATPPPY model (A), close-up snapshot taken from phosphorylation lip and aromatic cluster in WTATPPPY model with important residues as sticks (B).

3.7 Mutant, Unphosphorylated, Nucleotide-free Simulations

Rmsd plot of whole protein belonging to unphosphorylated, nucleotide-free simulation of mutant Hog1 is given in Figure 3.24. Rmsd plot of the lip sequence of this model is also given in the same figure.

In Figure 3.24, from rmsd graphs we can see that overall protein and lip movements are continuing to happen.

When the initial and final geometries of MUT model are aligned, an rmsd of 8.888 Å is obtained. After C-terminal 91 residues are excluded in the rmsd calculations, rmsd value is reduced to 3.220 Å. This shows that majority of the conformational changes are occurring in the c-terminal unstructured region of the protein. Aligned initial and final geometries of MUT model are given in Figure 3.25 A.

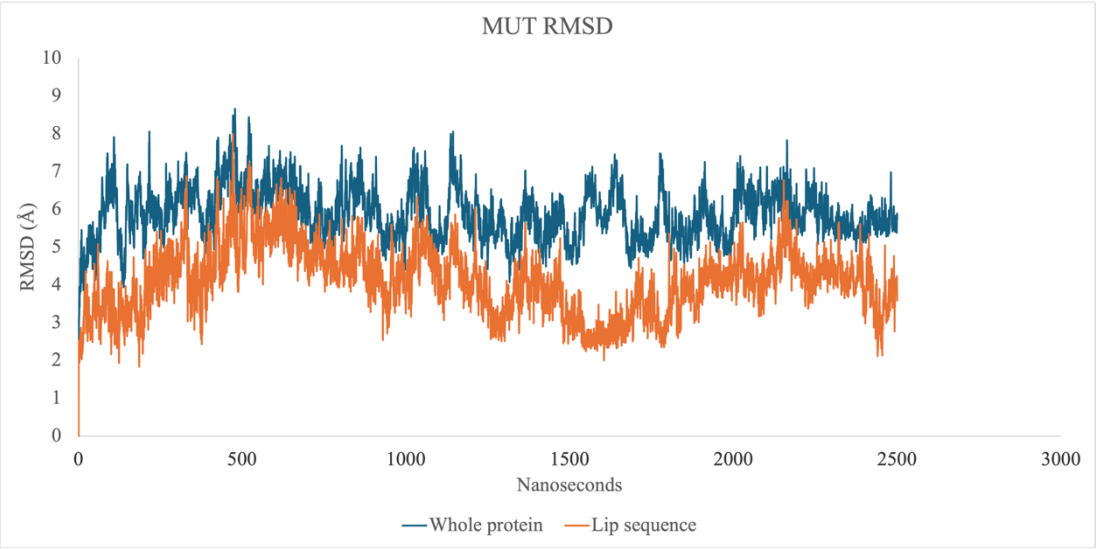

Figure 3.24: RMSD graph of whole protein (blue) and RMSD graph of lip sequence (orange) in MUT model.

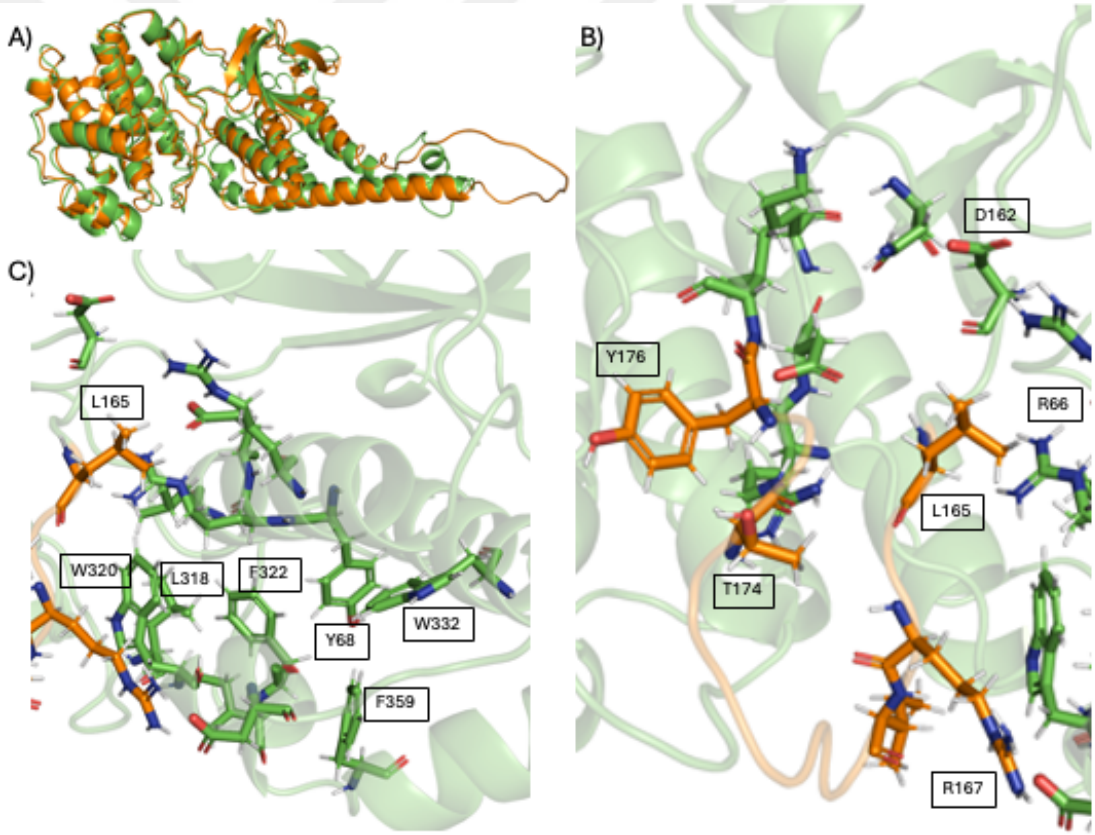

Figure 3.25: Alignment of initial and final geometries of MUT model (A), close-up snapshot taken from phosphorylation lip in MUT model with important residues as sticks (B), and close-up snapshot taken from hydrophobic cluster in MUT model with important residues as sticks (C).

In Figure 3.25 B, conformation of phosphorylation lip of MUT model resembles the WTATP model. L165 is moved towards the hydrophobic cluster, thus active site is open. However, L165 is not yet formed interactions seen in WTATP model.

In the final geometry, Figure 3.25 C, hydrophobic cluster of MUT model is shown. L165 is close to, but not in the hydrophobic cluster. Mutated residue L318 interacts with W320 and F322 residues.

3.8 Mutant, Unphosphorylated, ATP Bound Simulations

Rmsd plots of three unphosphorylated, ATP bound simulations of mutant Hog1, and corresponding lip sequences are given in Figures 3.26, 3.28 and 3.30.

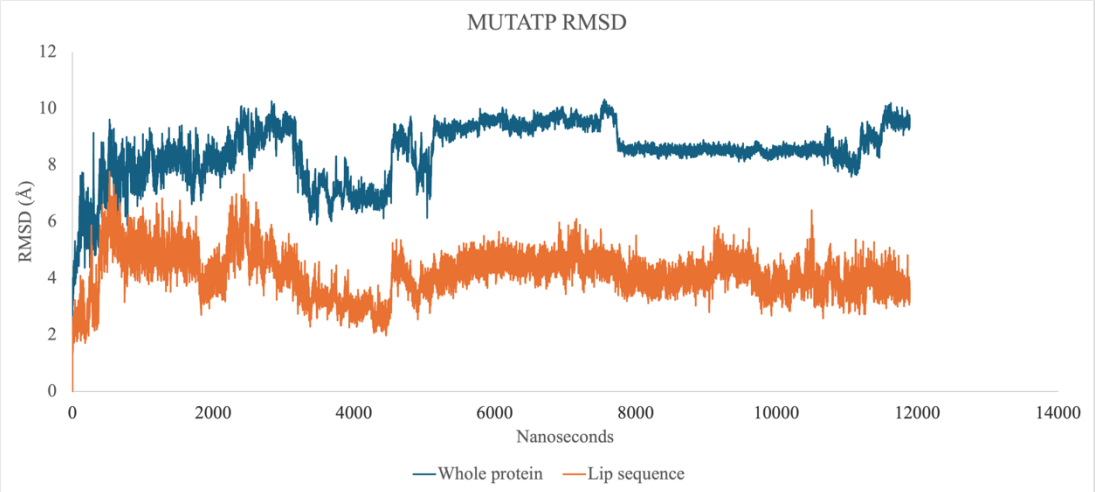

Figure 3.26: RMSD graph of whole protein (blue) and RMSD graph of lip sequence (orange) in MUTATP model.

In Figure 3.26, a conformational change can be observed in the overall protein at 7.5 μs, where lip sequence shows a change in the conformation close to 10 μs time point. After this point, lip sequence reaches an equilibrium. However, the overall protein continues changing its conformation after 11 μs.

When the initial and final geometries of MUTATP model are aligned, an rmsd of 9.999 Å is obtained. After C-terminal 91 residues are excluded in the rmsd calculations, rmsd value is reduced to 2.369 Å. This shows that majority of the conformational changes are occurring in the c-terminal unstructured region of the protein. Aligned initial and final geometries of MUTATP model are given in Figure 3.27 A.

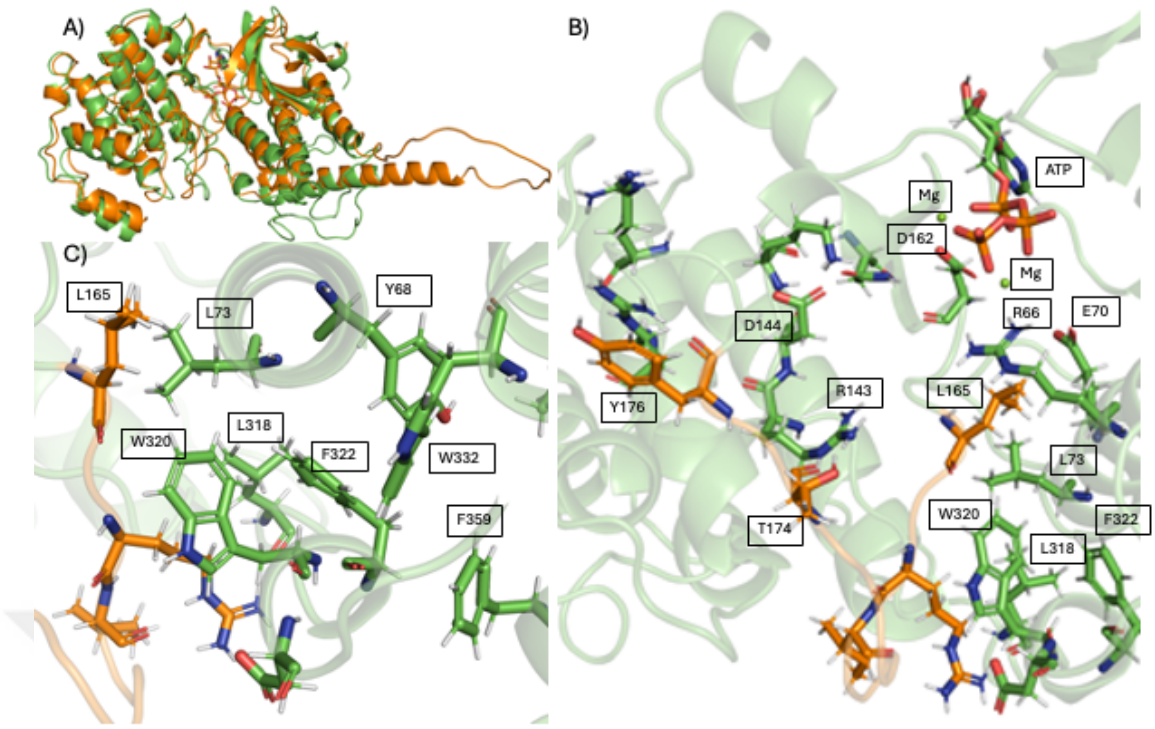

Figure 3.27: Alignment of initial and final geometries of MUTATP model (A), close-up snapshot taken from phosphorylation lip in MUTATP model with important residues as sticks (B), and close-up snapshot taken from hydrophobic cluster in MUTATP model with important residues as sticks (C).

In Figure 3.27 B, ATP is displaced from its initial position. E70 is contributing to the coordination shell of Mg^{2+} ion through water mediated interactions. D162 is directly involved in the coordination shell of Mg^{2+} ion. R66 is interacting directly with ATP, which could have an alternative catalytic effect in mutant model. Active site is open as in active form of the protein.

In Figure 3.27 C, L165 is moving towards the hydrophobic cluster and is interacting with L73, emptying the active site. W320 is interacting with L318. I168 is facing towards solvent and not blocking L165.

In the MUTATPY simulation, rmsd graph of overall protein and lip show change in the conformation at 5 μs (Figure 3.28).

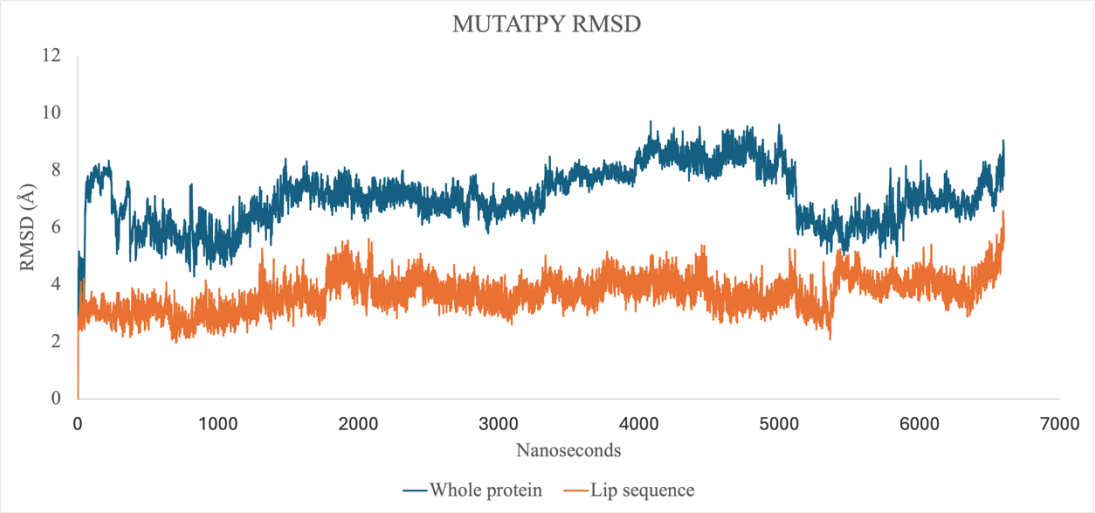

Figure 3.28: RMSD graph of whole protein (blue) and RMSD graph of lip sequence (orange) in MUTATPY model.

When the initial and final geometries of MUTATPY model are aligned, an rmsd of 8.255 Å is obtained. After C-terminal 91 residues are excluded in the rmsd calculations, rmsd value is reduced to 2.443 Å. This shows that majority of the conformational changes are occurring in the c-terminal unstructured region of the protein. Aligned initial and final geometries of MUTATPY model are given in Figure 3.29 A.

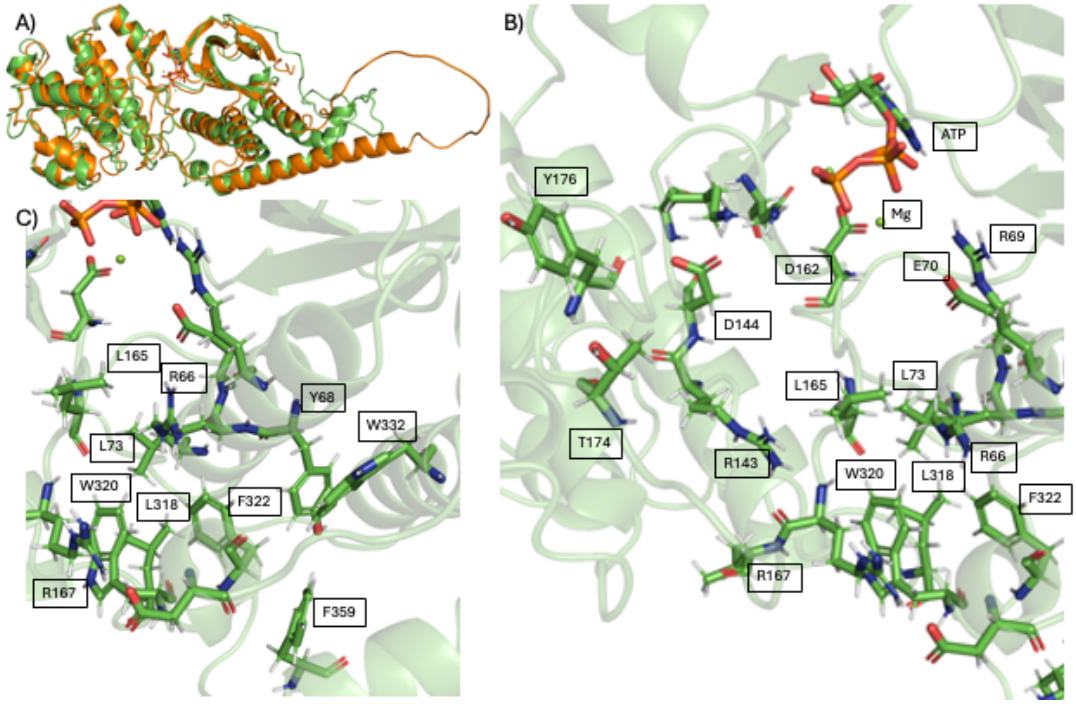

Figure 3.29: Alignment of initial and final geometries of MUTATPY model (A), close-up snapshot taken from phosphorylation lip in MUTATPY model with important residues as sticks (B), and close-up snapshot taken from hydrophobic cluster in MUTATPY model with important residues as sticks (C).

Figure 3.29 B shows the phosphorylation lip. T174 and Y176 are oriented away from the active site, leaving the active site open. L165 is also faced away from the active site, turned towards the hydrophobic cluster and enables an active site-open conformation. D162 contibutes to the coordination shell of Mg^{2+} ions directly, whereas E70 is involved in the coordination of Mg^{2+} through water mediated interactions.

In Figure 3.29 C, L165 is facing towards the hydrophobic cluster, however, is not yet interacting with the cluster. L165 faces R66 in the close proximity of hydrophobic cluster. Even though positioning itself near the hydrophobic cluster, it seems L165 still couldn't find its final position. Although manually manipulated towards solvent, W320 oriented its position back into the hydrophobic cluster, its original position.

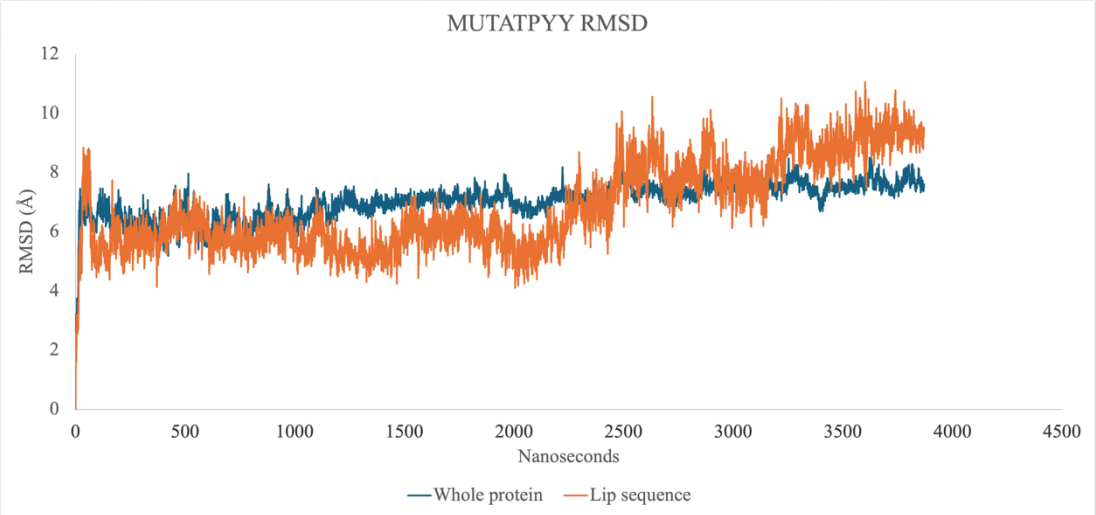

Figure 3.30: RMSD graph of whole protein (blue) and RMSD graph of lip sequence (orange) in MUTATPYY model.

Figure 3.30 shows rmsd plot of overall protein and lip sequence in MUTATPYY model. Both overall protein and lip show a change in conformation after 2 μs.

When the initial and final geometries of MUTATPYY model are aligned, an rmsd of 7.687 Å is obtained. After C-terminal 91 residues are excluded in the rmsd calculations, rmsd value is reduced to 2.956 Å. This shows that majority of the conformational changes are occurring in the c-terminal unstructured region of the protein. Aligned initial and final geometries of MUTATPYY model are given in Figure 3.31 A.

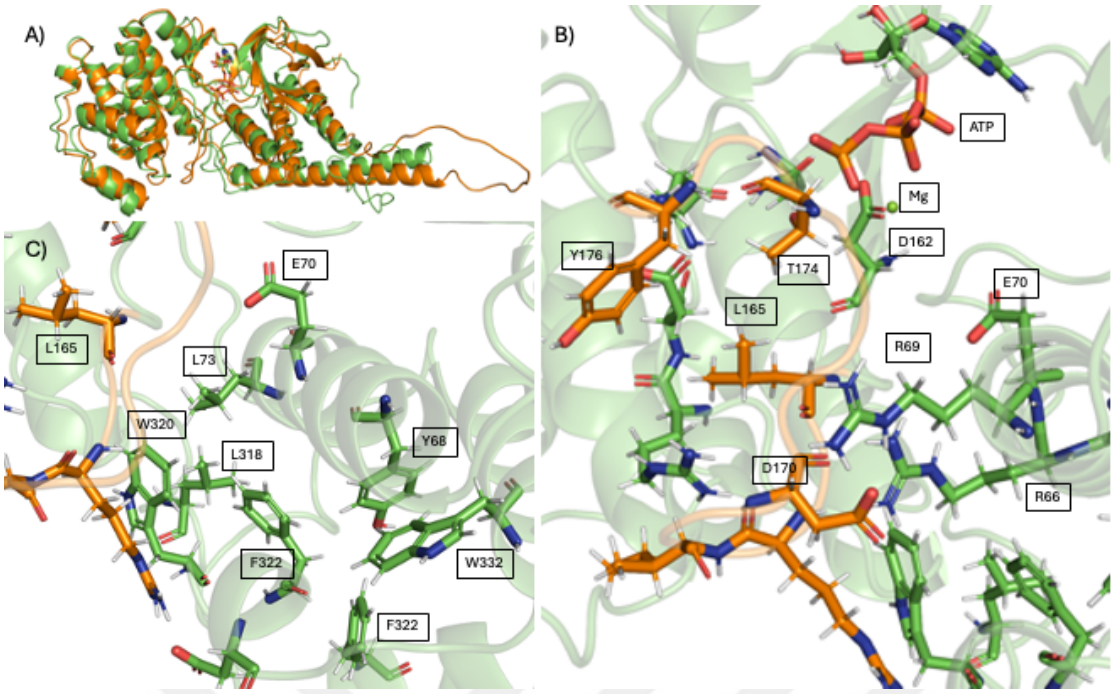

Figure 3.31: Alignment of initial and final geometries of MUTATPYY model (A), close-up snapshot taken from phosphorylation lip in MUTATPYY model with important residues as sticks (B), and close-up snapshot taken from hydrophobic cluster in MUTATPYY model with important residues as sticks (C).

In Figure 3.31 B, final geometry of phosphorylation lip in MUTATPYY model is shown. T174 interacts with gamma phosphate oxygen of ATP through its side chain OH group. E70 participates in the coordination shell of Mg^{2+} ion through water mediated contacts. R69 interacts with D170. R66 also interacts with D170, which stabilizes the region. Even though Y176 turned away from the active site, since T174 interacts closely with the gamma phosphate of ATP molecule, active site is highly occupied and in a close form.

In Figure 3.31 C, final geometry of the hydrophobic cluster in MUTATPYY model is shown. L165 is facing towards the lip, away from the hydrophobic cluster. This prevents L165 from interacting with the L318 or L73. Although manually turned towards solvent at the beginning of the simulation, F322 oriented itself back in its original position, thus participating in the hydrophobic cluster.

4. DISCUSSION

The structure given by Alphafold is similar to 1wfc (p38) and 1atp (cAMP-dependent protein kinase) crystal structures. There is a substrate analog in 1atp crystal. Alanine in the substrate analogue will be threonine or serine in the substrate, this residue is in between Phe187, which is the equivalent of Leu165 in Hog1, and ATP. In our Alphafold structure, L165 is in the same position as F187 in 1atp. In 1wfc, L74 makes hydrophobic interactions with Y323. We have L73 and F318 residues in the same position and they have the same interaction in the Alphafold structure. W320 residue in the wild type unphosphorylated, nucleotide-free system (WT), turns into the solvent around 2 μs. W320 interacts hydrophobically with F318 and L73 in Alphafold, preventing hydrophobic residues such as L165 or I168 from approaching L73. At 3 μs, I168 replaces W320 and interacts with L73, F318 shifts slightly to allow I168 to form above interactions. I355 makes hydrophobic contact with F318. Thus, a hydrophobic cluster different from Alphafold is formed in that region. In addition, D354 establishes a salt bridge with K72. Therefore, the 354-355 region, which is disordered in Alphafold, becomes a helix in the final structure and interacts more strongly with the hydrophobic cluster, which it was initially included in only through F359. All these interactions do not exist in other crystals. Structure of Erk2 (pdb crystals 1erk, 2erk) and structure of p38 (pdb: 1cm8) is similar to Alphafold predicted structure of HOG1 protein. Only in nucleotide-free, unphosphorylated p38 (1wfc), the region corresponding to L165-I168 is not visible, which means it is very mobile. In our simulation, the inclusion of I168 in the hydrophobic cluster brings L165 slightly closer to the active site than 1erk, 1atp and 1cm8. This may make substrate binding difficult. Other unphosphorylated, nucleotide-free wild-type simulations are 1 μs long and look similar to Alphafold predicted structure. This resemblence of similarity of models could stem from inadequate simulation time, since these models are simulated for short simulation times. If extended, they may also undergo conformational changes explained above, or there may be an equilibrium between the Alphafold structure and the newly formed structure. In order to say this for sure, these simulations need to be further extended. In one of the 2 dual phosphorylated, nucleotide-free simulations of

wild-type protein (WTPPEKLE), W320 turns towards solvent around 1 μs and I168 fills its place. However, the other changes mentioned are not seen in the double phosphorylated model. Considering that the simulation period is very short and that it takes several hundred ns for other changes to occur after W320 turns towards the solvent in the unphosphorylated state, similar changes may occur in phosphorylated case when simulations are further extended. L165 is also close to the active site, as in the unphosphorylated structure. The wild type non-phosphorylated ones with ATP behave similarly to each other in the hydrophobic cluster and they all resemble Alphafold. In WTATPY model, even if W320 is manually changed to face towards the solvent at the beginning of the simulation, it turns back to its original position inside the hydrophobic cluster. Likewise, when the F322 is manually manipulated to face to a different direction, this residue first turns into solvent, but after 4 μs, it returns to its place in the initial Alphafold structure. Therefore, the presence of ATP appears to favor the hydrophobic cluster in the Alphafold, not allowing an alternative cluster. The reasons for this should be investigated in the future. Presumably, ATP pulls the helix where L73 is located, reducing the compression of F318. But we don't have data to say this for sure yet. In all simulations with unphosphorylated wild-type ATP bound models, L165 moved away from the active site and towards the hydrophobic cluster. In the two longer simulations, L165 started to interact with W320. But W320 prevents L165 from interacting with L73 or F318, hence L165 cannot penetrate well into the hydrophobic cluster. Thus, the area between L165 and D162, which binds ATP, assumes a straight conformation. If L165 has a role in substrate positioning like 1atp, it is not possible for it to do it this way. In the 3rd simulation, which is only 4 μs, L165 moves away from the active region, but it has not yet reached the place seen in the other two ATP bound WT simulations. Assuming that this will go to the same final geometry as the others over time, we can say that in the presence of ATP, L165 residue in wild type unphosphorylated Hog1 will be insufficient to bind substrate or direct it for catalysis, since it is far from the active site. When compared to 1cm8 and 2erk, T174 and Y176 residues of one of the double phosphorylated, ATP bound wild type models (WTATPPPY) appear to bind to each other's binding sites. It is not possible for this to be an active structure because the active region is completely closed. It is necessary to extend the simulation to investigate if T174 and Y176 will be placed to their correct places. In the other double phosphorylated, ATP bound wild-type Hog1 structure (WTATPPP), T174 is in the same place as 1cm8 and 2erk. Y176 is close to

that in other crystals, but not in exactly the same place. In this structure, L165 is facing the active site, although not as much as unphosphorylated nucleotide-free wild-type model. The rest of the hydrophobic cluster is similar to Alphafold structure. In one of the unphosphorylated, ATP bound mutants (MUTATP), L165 again moves away from the active site. But unlike the wild type, L165 interacts with L73 and L318, with W320 shifting slightly. In this structure, ATP is also reoriented and a potentially catalytic interaction frequently occurs between beta phosphate and R66. Since this simulation was at high temperature, ATP may have moved due to high temperature conditions of the simulation. But in other simulations at high temperatures, such displacement of ATP does not occur. Additionally, ATP reorientation occurs after L165 makes hydrophobic contact with L73 and L318. This suggests that there is a connection between these two events. But it is not clear what causes this connection. Alternative models for this connection should be investigated in the future. On the other hand, the repositioning of L165 puts G164 in the same location as the side chain of F187 in 1atp. This suggests that L165 can perform the substrate positioning task in the wild type, while G164 can perform the substrate positioning task in the mutant. In the simulation with another ATP bound mutant model, L165 approaches the hydrophobic cluster but does not enter it. Since this simulation is at 303 K, events may be developing more slowly. The nucleotide-free mutant behaves similarly. The other ATP bound mutant simulation at 303 K only took 3.6 μs. L165 moved away from the active site but did not approach the hydrophobic cluster. Except for this short simulation, in the other mutant simulations, W320 faces the hydrophobic region, and even if its position is manually manipulated to face towards solvent, it comes back facing to the hydrophobic cluster after a while.

To sum up, in the unphosphorylated wild type model, L165 is very close to the active site when ATP is not present, but is very far away when ATP is present. Phosphorylation may serve to position L165 correctly. The mutant may position L165 in the hydrophobic cluster, replace it with G164, and position ATP in a different orientation, making it suitable for the reaction.

5. CONCLUSION

First finding in this study is Alphafold is successful in predicting the structure of Hog1 protein. After alignments of the Alphafold predicted structure of Hog1 with crystal structures of similar MAPK proteins 1erk and 2erk were made, rmsd analysis showed that Alphafold structure is in accordance with crystal structures. After excluding the C-terminal 91 residues from Alphafold predicted structure, where Alphafold refers as low reliable conformation due to lack of crystals containing this sequence, rmsd value was even lower from the initial value, which tells us the similar part of the sequence is predicted accurately by Alphafold.

Second, the position of Leu165 seems to be related to the substrate binding by Hog1. Since this residue is involved in positioning the substrate next to ATP, it should not move away from the active site. However, in ATP bound, unphosphorylated, wild type simulations it leaves the active site and move toward the hydrophobic cluster. In the wild type, phosphorylation seems to reposition Leu165 in the active site. On the other hand, in the mutant, Leu165 is situated deep inside the hydrophobic cluster next to Leu318. This arrangement relocates Gly175 in a position suitable for guiding the substrate in the active site. In addition, ATP acquires an alternative orientation. All together, these differences with respect to the wild type can explain why the mutant is constitutively active. To better understand, simulations should be extended.

Lastly, these models could provide data to understand the mechanisms in other organisms. Different engineering methods might be developed to manipulate the mutant protein, allowing us to activate or deactivate when needed. Also, inhibitory mechanisms or substrates might be developed by understanding the constitutive activation mechanism.

6. FUTURE WORKS

Current simulations should be extended to fully discover the events that are going to lead the mutation to show its effect in constitutive activation of the protein. Alternative mutations on interaction partners of key residues should be introduced to further investigate and validate the mechanism which mutation shows its effects. Also, experimental work points out to an autophosphorylation possibility in the mutant protein. This option is also should be investigated through future simulations.

REFERENCES

Bell, M., Capone, R., Pashtan, I., Levitzki, A., & Engelberg, D. (2001). Isolation of Hyperactive Mutants of the MAPK p38/Hog1 That Are Independent of MAPK Kinase Activation. *Journal of Biological Chemistry*, 276(27), 25351–25358. https://doi.org/10.1074/jbc.m101818200

Bellon, S., Fitzgibbon, M. J., Fox, T., Hsiao, H. M., & Wilson, K. P. (1999). The structure of phosphorylated P38γ is monomeric and reveals a conserved activation-loop conformation. *Structure*, *7*(9), 1057–1065. https://doi.org/10.1016/s0969-2126(99)80173-7

Blomberg, A. (2022). Yeast osmoregulation – glycerol still in pole position. *FEMS Yeast Research*, 22(1). https://doi.org/10.1093/femsyr/foac035

Canagarajah, B. J., Khokhlatchev, A., Cobb, M. H., & Goldsmith, E. J. (1997). Activation Mechanism of the MAP Kinase ERK2 by Dual Phosphorylation. *Cell*, *90*(5), 859–869. https://doi.org/10.1016/s0092-8674(00)80351-7

Çakar, Z. P., Turanlı-Yıldız, B., Alkım, C., & Yılmaz, L. (2011). Evolutionary engineering of Saccharomyces cerevisiae for improved industrially important properties. *FEMS Yeast Research*, *12*(2), 171–182. https://doi.org/10.1111/j.1567-1364.2011.00775.x

Hohmann, S. (2002). Osmotic stress signaling and osmoadaptation in yeasts. *Microbiology and Molecular Biology Reviews*, 66(2), 300-372. doi: 10.1128/MMBR.66.2.300-372.2002

Holyavkin C, Turanlı-Yıldız B, Yılmaz Ü, Alkım C, Arslan M, Topaloğlu A, Kısakesen Hİ, de Billerbeck G, François JM & Çakar ZP (2023) Genomic, transcriptomic, and metabolic characterization of 2-Phenylethanol-resistant Saccharomyces cerevisiae obtained by evolutionary engineering. *Front. Microbiol*. 14:1148065. doi: 10.3389/fmicb.2023.1148065

Jacoby, T., Flanagan, H., Faykin, A., Seto, A. G., Mattison, C., & Ota, I. (1997). Two Protein-tyrosine Phosphatases Inactivate the Osmotic Stress Response Pathway in Yeast by Targeting the Mitogen-activated Protein Kinase, Hog1. *Journal of Biological Chemistry*, 272(28), 17749–17755. https://doi.org/10.1074/jbc.272.28.17749

O'Rourke, S. M., & Herskowitz, I. (1998). The Hog1 MAPK prevents cross talk between the HOG and pheromone response MAPK pathways in Saccharomyces cerevisiae. *Genes & Development*, 12(18), 2874–2886. https://doi.org/10.1101/gad.12.18.2874

Proft, M., & Struhl, K. (2004). MAP kinase-mediated stress relief that precedes and regulates the timing of transcriptional induction. *Cell*, 118(3), 351-361. doi: 10.1016/j.cell.2004.07.032

Saito, H., & Posas, F. (2012). Response to hyperosmotic stress. *Genetics*, 192(2), 289-318. doi: 10.1534/genetics.112.140863

Shiozaki, K., & Russell, P. (1995). Cell-cycle control linked to extracellular environment by MAP kinase pathway in fission yeast. *Nature*, 378(6552), 739-743. doi: 10.1038/378739a0

Westfall, P. J., & Thorner, J. (2006). Analysis of mitogen-activated protein kinase signaling specificity in response to hyperosmotic stress: Use of an analog-sensitive HOG1 allele. *Eukaryotic Cell*, 5(1), 1215-1228. doi: 10.1128/EC.00128-06

Westfall, P. J., Patterson, J. C., Chen, R. E., & Thorner, J. (2008). Stress resistance and signal fidelity independent of nuclear MAPK function. *Proceedings of the National Academy of Sciences*, 105(34), 12212-12217. doi: 10.1073/pnas.0806621105

Zheng, J., Trafny, E. A., Knighton, D. R., Xuong, N., Taylor, S. S., Ten Eyck, L. F., & Sowadski, J. M. (1993) 2.2 Å refined crystal structure of the catalytic subunit of cAMP-dependent protein kinase complexed with MnATP and a peptide inhibitor. *Acta Crystallographica Section D Biological Crystallography*, 49(3), 362–365. https://doi.org/10.1107/s0907444993000423

CURRICULUM VITAE

Name Surname **:** Altuğ ULUDAĞ

EDUCATION **:**

- **B.Sc.** **:** 2017, Istanbul Technical University, Faculty of Science and Letters, Molecular Biology and Genetics Department